RECLAMATION
Managing Water in the West

Desalination and Water Purification Research
and Development Program Report No. 213

Nanophotonic Pervaporation Desalination

U.S. Department of the Interior
Bureau of Reclamation
Technical Service Center
Denver, Colorado

January 2018

REPORT DOCUMENTATION PAGE		*Form Approved* *OMB No. 0704-0188*

The public reporting burden for this collection of information is estimated to average 1 hour per response, including the time for reviewing instructions, searching existing data sources, gathering and maintaining the data needed, and completing and reviewing the collection of information. Send comments regarding this burden estimate or any other aspect of this collection of information, including suggestions for reducing the burden, to Department of Defense, Washington Headquarters Services, Directorate for Information Operations and Reports (0704-0188), 1215 Jefferson Davis Highway, Suite 1204, Arlington, VA 22202-4302. Respondents should be aware that notwithstanding any other provision of law, no person shall be subject to any penalty for failing to comply with a collection of information if it does not display a currently valid OMB control number.
PLEASE DO NOT RETURN YOUR FORM TO THE ABOVE ADDRESS.

1. REPORT DATE *(DD-MM-YYYY)* January 2018	2. REPORT TYPE Final	3. DATES COVERED *(From - To)* September 2016 – December 2017

4. TITLE AND SUBTITLE Nanophotonic Pervaporation Desalination: Modeling and experiments of advanced hybrid pervaporation membrane processes to minimize concentrate volume for inland brackish water desalination	5a. CONTRACT NUMBER Agreement No. R16AC00125
	5b. GRANT NUMBER
	5c. PROGRAM ELEMENT NUMBER
6. AUTHOR(S) Mary Laura Lind, Shane Walker, Matthew Green, and Stewart Mann	5d. PROJECT NUMBER
	5e. TASK NUMBER
	5f. WORK UNIT NUMBER

7. PERFORMING ORGANIZATION NAME(S) AND ADDRESS(ES) Dr. Mary Laura Lind Arizona Board of Regents on behalf of Arizona State University P.O. Box 875011 Tempe, AZ 85287-6011	8. PERFORMING ORGANIZATION REPORT NUMBER

9. SPONSORING/MONITORING AGENCY NAME(S) AND ADDRESS(ES) Bureau of Reclamation U.S. Department of the Interior Denver Federal Center PO Box 25007, Denver, CO 80225-0007	10. SPONSOR/MONITOR'S ACRONYM(S) Reclamation
	11. SPONSOR/MONITOR'S REPORT NUMBER(S) DWPR Report No. 213

12. DISTRIBUTION/AVAILABILITY STATEMENT
Available from the National Technical Information Service,
Operations Division, 5285 Port Royal Road, Springfield VA 22161

13. SUPPLEMENTARY NOTES
Online at https://www.usbr.gov/research/dwpr/DWPR_Reports.html

14. ABSTRACT

This research focused on evaluating concentration polarization in a hybrid reverse osmosis/pervaporation system for managing inland brackish water desalination concentrate through computational analysis and experiments. Concentration polarization is more significant in pervaporation than in reverse osmosis. The propensity for scaling based on activities is lower than that based on concentrations and can be mitigated when necessary by adjusting residence time or adding antiscalents. The secondary focus was developing flux-enhanced nanophotonic pervaporation membranes. The photothermal effect resulted in up to 69% enhancement in flux in the first-generation nanophotonic membranes for recovery of brackish waters, with chloride rejections greater than 99.9%. The photothermal effect also has the potential to mitigate concentration polarization in pervaporation.

15. SUBJECT TERMS
Pervaporation, nanophotonic, reverse osmosis, scaling, concentration polarization

16. SECURITY CLASSIFICATION OF:			17. LIMITATION OF ABSTRACT	18. NUMBER OF PAGES	19a. NAME OF RESPONSIBLE PERSON Yuliana Porras Mendoza
a. REPORT U	b. ABSTRACT U	THIS PAGE U			19b. TELEPHONE NUMBER *(Include area code)* 303-445-2265

Standard Form 298 (Rev. 8/98)
Prescribed by ANSI Std. Z39.18

Nanophotonic Pervaporation Desalination: Modeling and Experiments of Advanced Hybrid Pervaporation Membrane Processes to Minimize Concentrate Volume for Inland Brackish Water Desalination

by

Mary Laura Lind*, Shane Walker, Matthew Green*, and Stewart
Mann***

***School for Engineering of Matter, Transport, and Energy
Arizona State University
Tempe, Arizona**

****Department of Civil and Environmental Engineering
University of Texas at El Paso
El Paso, Texas**

Mission Statements

The U.S. Department of the Interior protects America's natural resources and heritage, honors our cultures and tribal communities, and supplies the energy to power our future.

The mission of the Bureau of Reclamation is to manage, develop, and protect water and related resources in an environmentally and economically sound manner in the interest of the American public.

Disclaimer

The views, analysis, recommendations, and conclusions in this report are those of the authors and do not represent official or unofficial policies or opinions of the United States Government, and the United States takes no position with regard to any findings, conclusions, or recommendations made. As such, mention of trade names or commercial products does not constitute their endorsement by the United States Government.

Acknowledgments

Acronyms and Abbreviations

BGNDRF   Brackish Groundwater Desalination Research Facility
CB   carbon black
CCD™   Closed-circuit desalination
CERRO™   Batch recycling of concentrate
DCMD   direct contact membrane distillation
IPAB   Industrial Practitioners Advisory Board
LED   light-emitting diode
LHS   left hand side
MD   membrane distillation
NESMD   nanophotonic-enabled solar membrane distillation
NEWT   Nanotechnology Enabled Water Treatment
NP   nanoparticles
PFDF   poly vinylidene fluoride
PDMS   polydimethylsiloxane
PVA   polyvinyl alcohol
Reclamation   Bureau of Reclamation
RHS   right hand side
RIS   resistance in series
RO   reverse osmosis
SBLMTC   solute boundary layer mass transfer coefficient
SEM   scanning electron microscope
SWCNT   single walled carbon nanotube
TDS   total dissolved solids
TFBLT   thin film boundary layer theory
THF   tetrahydrofuran
UV   ultraviolet
VMD   vacuum membrane distillation
VOC   volatile organic compounds
WMTC   water mass transfer coefficient

Measurements

[]   dimensionless
$°C$ degree Centigrade
$°F$ degree Fahrenheit
cm   centimeter
cm^2 square centimeters
cm^3 cubic centimeter
$cm^3 \, s^{-1}$ cubic centimeters per second (volumetric flow)
dz One increment (0.1 meter [m]) along axis of flow
g   gram
$g \, cm^{-3}$ grams per cubic centimeter (mass concentration)
g/L   grams per liter
$g \, L^{-1}$ grams per liter
$g \, s^{-1}$ grams per second (mass flow rate)
J   Joule
$J \, mol^{-1}$ Joules per mole
$J \, g^{-1} \, K^{-1}$ Joules per gram per degree Kelvin
$J \, kg^{-1}$ Joules per kilogram
$J \, mol^{-1} \, K^{-1}$ Joules per mole per degree Kelvin
$J \, s^{-1}$ Joules per second

Nanophotonic Pervaporation Desalination

K	degree Kelvin
kg m^{-3}	kilograms per cubic meter (mass concentration)
kg m^{-1} s^{-1}	kilograms per meter per second (viscosity)
kg m^{-2} h^{-1}	kilograms per meter squared hour (flux)
kg m^{-2} s^{-1}	kilograms per square meter per second (flux)
kg m^{-2} s^{-1} kPa^{-1}	kilograms per square meter per second per kilopascal (permeance)
kPa	kilopascal
kW/kg h	kilowatts per kilograms per hour
L bar mol^{-1} K^{-1}	liter-bars per mole per degree Kelvin (gas constant R)
L m^{-2} h^{-1}	liters per square meter per hour (volumetric flux)
L m^{-2} h^{-1} bar^{-1}	liters per square meter per hour per bar (water mass transfer coefficient)
M	Molar
m h^{-1}	meters per hour (solute mass transfer coefficient)
M/L	moles per liter
m s^{-1}	meters per second (feed channel velocity,v, or volumetric water flux, v')
m^2 s^{-1}	square meters per second (solute diffusion coefficient)
m^3	cubic meter
m^3 s^{-1}	cubic meters per second (feed volumetric flow)
mg/L	milligrams per liter
mg L^{-1}	milligrams per liter
mg s^{-1}	milligrams per second (solute transmembrane mass transfer rate)
mg m^{-2} h^{-1}	milligrams per square meter per hour (solute flux)
mg m^{-3}	milligrams per cubic meter (mass concentration)
mm	millimeter
mol L^{-1}	moles per liter
mol m^{-2} s^{-1}	moles per square meter per second (molar flux, J_i)
mol^2 m^{-2} s^{-1} J^{-1}	square moles per square meter per second per Joule
mol m^{-2} s^{-1} kPa^{-1}	moles per square meter per second per kilopascal
mol m^{-2} s^{-1} Pa^{-1}	moles per square meter per second per Pascal
mol m^{-3}	moles per cubic meter (molar concentration)
nm	nanometer
s^{-1}	inverse second (feed impeller rotational (angular) speed)
s m^{-1}	seconds per meter (reciprocal solute boundary layer mass transfer coefficient)
W m^{-2}	Watts per square meter
W m^{-2} K^{-1}	Watts per square meter per degree Kelvin
wt%	percent weight
μm	micrometer
μg/L	micrograms per liter

Variables

A and b	ion specific parameters
a	activity
C	ion concentration
C_F	solute feed concentration
c_i	concentration of species i in the boundary layer
c_{ib}	bulk solute feed concentration
c_{i0}	concentration of species i at the feed membrane interface
C_P	solute permeate concentration
C'	concentration polarization modulus
Δ	boundary layer thickness
dc_i	boundary layer change in solute concentration
d_H	hydraulic diameter
D_i	solute mass diffusion coefficient
D_{NaCl}	solute diffusion coefficient
dz	feed channel incremental length
E	enrichment
E_A	activation energy of permeation
E_0	intrinsic enrichment
$F_{i,total}$	total permeance of species i
h	feed channel height
h_L	head loss
h_0	boundary layer heat transfer coefficient
I	ionic strength
J	VOC flux
J	water flux
J	flux
J_i	the molar flux of species i
$J_{s,z}$	the solute flux
J_w	water flux
$J_{w,z}$	incremental water flux
k_{cp}	solute boundary layer mass transfer coefficient
k_0	SBLMTC $\frac{D_i}{\delta}$ in the RIS model
k_s	solute membrane mass transfer coefficient
k_{SH}	Sherwood SBLMTC
k_w	membrane water mass transfer coefficient (an assumed constant)
l	membrane thickness
$M_{s,z}$	solute transmembrane mass transfer rate
m	boundary layer
P	total permeate pressure
Pe	Peclet number
P_F	hydraulic feed pressure
p_m	water vapor pressure at the feed/membrane interface
P_P	hydraulic permeate pressure
P_w^{sat}	feed side water saturation pressure
$\mathbb{P}_m$	is the water permeance of the membrane
R	gas constant
Q	heat flow to the bulk feed
Q_f	feed volumetric flow
$Q_{i,int}$	intrinsic membrane permeability of species i
q_p	plasmonic heat flux
$\left(q_{f,out} - q_{f,in}\right)$	heat flux through the liquid feed stream

Nanophotonic Pervaporation Desalination

Q_P	permeate flow rate
q_r	heat flux due to irradiation from the UV lamp
q_v	heat flux required to vaporize water
Re	Reynolds number
Rej	rejection
Sc	Schmidt number
Sh	Sherwood number
T	temperature [K]
T_b	bulk feed temperature
T_m	temperature at the feed/membrane interface,
T_p	permeate side temperature [K]
v_z	feed velocity
v'	volumetric water flux
w	feed channel width
x	length dimension normal to membrane at the boundary layer
x_i	ion mole fraction
x_w	feed side liquid water mole fraction
γ	activity coefficient
y_w	permeate side vapor phase water mole fraction
z	ion valence
α, β	empirical exponents
a and γ	fitting parameters
ΔH	enthalpy change of the bulk feed
ΔH_v	enthalpy change of vaporization for the permeating species
ℙ	intrinsic membrane permeability
ρ	water density
δ	boundary layer thickness
δ_{HL}	head loss coefficient
μ	water viscosity
γ	activity coefficient
γ_w	water activity coefficient
π	osmotic pressure
ω	feed impeller rotational speed
φ	transmembrane heat flux

Contents

Figures

Tables

Executive Summary

Surface and groundwaters have increasing concentrations of salts from agriculture and water softening activities—particularly in the arid southwestern part of the United States, increasing the need for inland brackish water desalination. Managing the concentrated waste produced through desalination (including minimization, treatment, and disposal solutions) is an ongoing critical challenge to inland brackish water desalination. During inland brackish groundwater desalination, disposal of the concentrate can often constrain the design and overall feasibility. Reverse osmosis (RO) is typically used to achieve 75 to 85% recovery of the feed water. The maximum recovery is typically limited by sparingly soluble salts (e.g., calcium sulfate) or minerals (e.g., silica) and, ultimately, depends on the feed water composition. The objectives of this project were to:

1) Assess the viability of a combined desalination process using RO, followed by pervaporation to help minimize the concentrate volume for inland brackish groundwater

2) Investigate the performance of nanophotonic enhanced pervaporation membranes for desalination

Pervaporation is a membrane process that separates mixable liquids by a combination of liquid permeation through and vapor evaporation from a dense semi-permeable membrane. It uses hydrophilic dense nonporous (polymer membranes) or microporous (inorganic membranes), in which the driving forces are vapor pressure of the main permeating species and, indirectly, temperature. Pervaporation is similar to membrane distillation (MD). However, pervaporation involves evaporation through a dense membrane while MD involves evaporation though an openly porous, hydrophobic membrane. The dense nature of the pervaporation membrane precludes the significant challenges of MD membranes (wetting out and conductive heat loss through the membrane).

One of our original hypothesis was that as pervaporation is not a concentration limited process, pervaporation would enable higher water recovery than RO. We realized an important question was related to scaling. To investigate this, we performed detailed analysis of concentration polarization, which can cause water flux impairment and can contribute to scaling of separation membranes. Our investigation, based on analysis of previously published studies on pervaporation desalination using a variant of thin film boundary layer theory, showed concentration polarization moduli up to 100 (dimensionless); whereas the concentration polarization moduli in RO processes are usually between 1 and 2. This means that pervaporation desalination requires more attention to residence time and using antiscalants for high concentration pervaporation feeds. Later, our experiments demonstrated that it was possible to recover at least an additional 15% of the brackish water RO concentrates with antiscalants added.

Nanophotonic Pervaporation Desalination

Our second main hypothesis was that we could improve the pervaporation membrane performances (increase fluxes) by coating nanophotonic particles on the feed surfaces of the pervaporation membranes. In the context of our work, nanophotonics entails the interaction of nanoparticles with light. Nanoparticles of surface-plasmon-resonant noble metals, semiconductors, and carbon can exhibit photothermal effects. This means that the nanoparticles heat up when exposed to light. Nanophotonic materials can directly convert solar energy into thermal energy with efficiencies up to 80%.

We coated carbon black nanoparticles onto the feed surfaces of commercially available asymmetric polyvinyl alcohol (PVA) membranes (designed for dehydration of alcohols and organics). We tested these membranes in a flat-sheet, cross-flow pervaporation system with a clear feed-window using simulated brackish waters and brackish water concentrates from the Brackish Groundwater Desalination Research Facility (BGNDRF) well 3 and Buckeye, Arizona well water. Importantly, we found that our coating of nanophotonic carbon black particles did not significantly alter the conventional membrane pervaporation desalination performance. Under solar simulator irradiation, we found that nanophotonic coated membranes exhibited up to 69% increases in pervaporation desalination membrane flux (up to 37% from radiative effects and 33% from the photothermal effect. The photothermal effect is consistent with reports for nanophotonic enhanced membrane distillation membranes.

Our theoretical and computation research has indicated that nanophotonic heating of the membrane surface thins the concentration polarization layer. This will increase flux by increasing the mole fraction of the main permeating species in the boundary layer, and will also improve separation (e.g., salt rejection in desalination). This also implies that scaling will be reduced because of the decreased concentration polarization (i.e., decreased solute concentration in the boundary layer).

We recommend that, in addition to being used to treat water from concentrated inland brackish water RO brine solutions, future applications of nanophotonic enhanced pervaporation membranes be considered for other waters with solute concentrations that exceed the limits of RO (e.g., produced wastewaters), in decentralized environments, and for separations that are the main commercial use of pervaporation membranes because nanophotonic membranes are more energy efficient (less costly to operate). Two specific areas of future research to further improve nanophotonic enhanced pervaporation desalination are:

1) New dense pervaporation membranes that are actually optimized for desalination

2) Innovations designed to allow nanophotonic membranes to have access to direct-solar light

1. Introduction

Surface and groundwaters have increasing concentrations of salts from agriculture and water softening activities—particularly in the arid southwestern part of the United States, increasing the need for inland brackish water desalination. Managing the concentrated waste produced through desalination (including minimization, treatment, and disposal solutions) is an ongoing critical challenge to inland brackish water desalination. Disposal of the concentrate from inland brackish groundwater desalination, can often constrain the design and overall feasibility. Reverse osmosis (RO) is typically used to achieve 75 to 85% recovery of the feed water. The maximum recovery is typically limited by sparingly soluble salt (e.g., calcium sulfate) concentration, mineral (e.g., silica) concentration, and osmotic pressure of the feed. Unfortunately, this results in wasting 15 to 25% of the source water as concentrate, and the disposal of this concentrate is typically one of the more costly components of inland desalination systems. While some technologists have successfully demonstrated the use of closed-circuit desalination (CCD^{TM}) or batch recycling of concentrate (CERRO^{TM}) with RO systems, these technologies require increasing energy consumption that is almost proportional with increasing concentrate salinity.

Researchers have investigated various combinations of separation technologies for minimizing the concentrate volume of inland brackish water desalination. Attempts have even been made to turn the concentrate into a valuable resource. These include treating the concentrate from inland brackish water RO further with pressure driven membrane processes, thermal processes, or electrical-potential driven membranes. Pressure driven processes are limited by the solute concentration within the feedwaters (e.g., < 60,000 milligrams per liter [mg/L]) and are not suited to high concentrations because of both scaling and pressure limitations. Thermal membrane-based processes have the key advantage of robustly dealing with waters with very high salt concentrations (e.g., > 100,000 mg/L)—much higher than the capacity of osmotic processes. Our investigations have shown that scaling propensity is lower when chemical activities instead of concentrations are used as a predictor and depend more on kinetic (residence time) than thermodynamic constraints. However, conventional thermal processes are considered to be energy intensive.

Recently, developments in hydrophilic pervaporation membranes provide an opportunity for significantly decreasing the specific energy consumption of desalination. Pervaporation is a membrane process driven by chemical activity differences that separates mixable liquids by a combination of permeation and evaporation in a dense, semi-permeable membrane. Because the pervaporation process uses membranes, the operation temperatures are lower than the boiling point of the components that are separated (unlike processes such as distillation).

Nanophotonic Pervaporation Desalination

Our research on the development of nanophotonic enhanced pervaporation shows significant flux enhancement over conventional pervaporation. Nanophotonic enhanced pervaporation requires significantly less energy costs than conventional pervaporation because essentially the nanophotonic enhanced pervaporation feed is heated by sunlight (i.e., free energy). In addition to being enhanced by increasing feed vapor pressure, flux is also enhanced by an increase in water mole fraction at the feed and membrane interface as a consequence of the concentration polarization mitigation effect. Mitigating concentration polarization also will reduce the propensity for scaling since the solute mole fraction is decreased in the boundary layer.

Membrane distillation (MD) is similar to pervaporation desalination in that it is driven by the temperature-dependent differences in vapor pressure of the components being separated. However, MD uses porous hydrophobic membranes whose sole purpose is to provide a barrier between the liquid and vapor phases. The MD membrane does not exhibit selectivity for any specific dissolved component. Some researchers maintain that, in general, conventional MD can achieve higher water flux than conventional pervaporation desalination. This conclusion should be taken as preliminary because there are so few published studies on pervaporation desalination (see Table 2 and Table 7 later in this report).

Vacuum membrane distillation (VMD) has almost identical energy requirements as pervaporation desalination on the lab scale. For example, both processes require heating the feed and supplying the energy for the vacuum pump on the permeate side. A significant problem for VMD is that the membrane can become wet from applying the vacuum. Therefore, VMD is not being widely investigated for desalination applications, although it is the most energy efficient type of membrane distillation.

Direct contact membrane distillation (DCMD) is a more widely investigated form of MD than VMD. In DCMD, both the feed and permeate side of the membrane are in contact with liquid water, and the feed side is maintained at a higher temperature. A major problem with DCMD is that significant conductive heat (energy) loss can occur across the membrane from the water contact on both sides of the membrane. This makes DCMD less energy efficient than VMD or pervaporation desalination.

Nanophotonic materials can directly convert solar energy into thermal energy with efficiencies up to 80%. Recent developments have shown that coating DCMD membranes with nanophotonic materials reduces the specific energy consumption of the MD process. However, the relative efficiency of energy capture in DCMD compared to pervaporation desalination is not known, and may, in fact, be significantly less in DCMD due to conductive heat loss through the DCMD membrane.

Additionally, it is claimed (Martinez-Diez and Vazquez-Gonzalez 1999) that concentration polarization is minimal in DCMD. If this is true, then, flux enhancement due to mitigation of concentration polarization will also be minimal. This is in contrast to nanophotonic flux enhanced pervaporation desalination, where flux enhancement is due to both an increase in feed side vapor pressure and mitigation of concentration polarization.

Moreover, to date, non-enhanced MD is considered too energy intensive to be an effective concentrate management strategy. Table 1 shows a comparison between conventional and nanophotonic pervaporation membranes.

Table 1.—Comparison Conventional vs. Nanophotonic Pervaporation

Parameter	Conventional pervaporation	Nanophotonic pervaporation
Energy requirement to heat feed	electric heat source	solar
Flux	low	high
Scaling propensity	high	low
Uses	Ethanol dehydration	Ethanol dehydration RO concentrate recovery Stand-alone desalination

Based on the above considerations, we further investigated the potential for nanophotonic enhanced pervaporation for inland brackish water desalination concentration management.

Our preliminary analysis of experimental data on new superhydrophilic pervaporation membranes shows that the energy consumption of desalination with pervaporation has a specific energy consumption that is approximately 25% of (i.e., 75% less than) that of desalination with membrane distillation. Therefore, we further investigated the potential of pervaporation for inland brackish water desalination concentration management.

Alternatively, pervaporation is an exciting technology to consider for concentrate recovery because it is driven by a differential in water vapor pressure (chemical activity differences), which is much less sensitive to salinity than reverse osmosis (RO).

Only limited previous research has investigated pervaporation as a method for treatment of high salinity waters and brine management. Recent advances in membrane technology, including the development of hydrophilic polymers and nanophotonics, suggest that this integrated platform could provide the next breakthrough in concentrate management.

1.1. Project Needs and Objectives

1.1.1. Needs

During inland brackish groundwater desalination, disposal of the concentrate can often constrain the design and overall feasibility. RO is typically used to achieve 75 to 85% recovery of the feed water. The maximum recovery is typically limited by sparingly soluble salts (e.g., calcium sulfate) or minerals (e.g., silica) and, ultimately, depends on the feed water compositions. There is a need for new technological solutions to minimize concentrate production.

1.1.2. Objectives

The objectives of this project were to:

1) Assess the viability of a combined desalination process using RO, followed by pervaporation to help minimize the concentrate volume for inland brackish groundwater

2) Investigate the performance of nanophotonic enhanced pervaporation membranes for desalination

1.2. Project Background

1.2.1. Problem

Managing concentrate is a primary continuing challenge for desalination. This challenge becomes increasingly magnified in inland brackish water desalination. During inland brackish groundwater desalination, disposal of the concentrate often constrains the design and overall feasibility. RO typically achieves 75 to 85% recovery, which is typically limited by sparingly soluble salts (e.g., calcium sulfate) or minerals (e.g., silica) and depends on raw water composition. Unfortunately, this results in 15 to 25% of the source water being wasted. While some researchers have considered the use of closed-circuit desalination (CCD^{TM}) or batch recycling of concentrate (CERRO^{TM}) with RO systems, these systems require nearly proportional increases in energy consumption with higher concentrate salinity associated with higher recovery (Tarquin and Delgado 2012 and Desalitech 2016).

1.2.2. Pervaporation

1.2.2.1. Fundamentals of Pervaporation

Pervaporation is a membrane process which separates mixable liquids by a combination of liquid permeation through and vapor evaporation from a dense semi-permeable membrane (Wynn 2000). This phase change during pervaporation makes it a unique membrane process. Pervaporation is useful for separations that are difficult to perform by extraction, distillation, or sorption. The

selective pervaporation membrane enables separation of species at significantly lower temperatures than distillation.

Pervaporation has been primarily used for two distinct applications: (1) in dehydration applications, such as dehydration of alcohols such as ethanol and (2) in selective removal of hydrophobic molecules such as alcohol or organic solvents from dilute aqueous solutions (Wynn 2000, Shi et al. 2012, Kreiter et al. 2008, Yadav et al. 2013, and Le et al. 2011). Pure dense polymer membranes, pure porous inorganic membranes, and mixed-matrix membranes are currently used for pervaporation (Peng et al. 2010, Bowen et al. 2004, and Mulder et al. 1983). Pervaporation applications for dehydration use hydrophilic membranes which selectively transport water (e.g., cellulose acetate, polyvinyl alcohol, and zeolites etc.) while pervaporation applications for removing hydrophobic molecules from dilute aqueous solutions use hydrophobic membranes (e.g., polydimethyl siloxane, poly[1-trimethylsilyl-1-propyne], and hydrophobic zeolite imidazolate frameworks). One main benefit of pervaporation, as compared to distillation, is that pervaporation can break azeotropes.

Figure 1(a) depicts pervaporation from a process level and Figure 1(b) shows the mechanism of transport through the pervaporation membrane. Transport through dense, polymeric pervaporation membranes occurs through a solution-diffusion process (Wijmans and Baker 1995). This is where the permeability through the membrane is a function of both the solubility and the diffusivity of the different species within the dense polymer material.
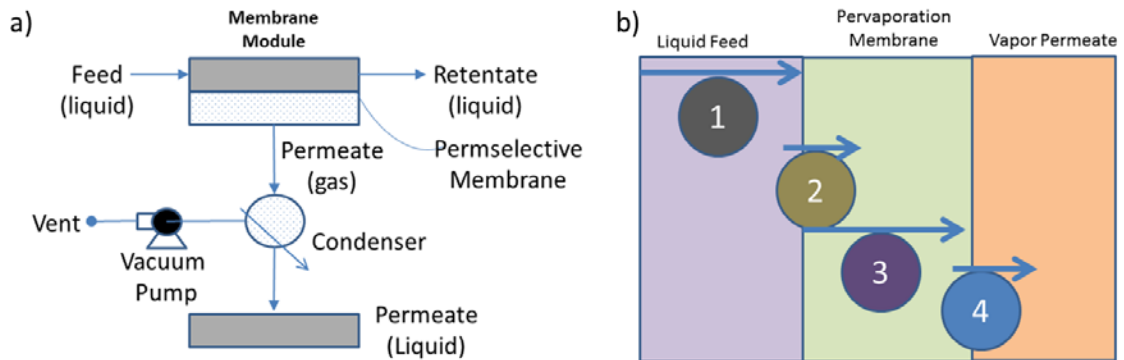
Figure 1—(a) Schematic of pervaporation process. (b)Schematic of details of transport within pervaporation process—step (1) transfer of the main permeating species from the bulk feed to the membrane surface, governed by the concentration gradient that exists between the bulk feed and the membrane surface (step 2) sorption of the permeating species onto the membrane surface; (step 3) is the diffusion of the main permeating species through nonporous membrane; (step 4) transfer of the main permeating species from the membrane surface on the permeate side to the bulk permeate.

Because pervaporation operates at temperatures much lower than processes like distillation, it a strong emerging candidate for managing waters with high total dissolved solids (TDS) concentrations such as inland brackish water desalination concentrates, seawater desalination concentrates, and fracking wastewater.

1.2.2.2. Distinction Between Pervaporation and Membrane Distillation

Water transport in pervaporation and MD is described by (Baker 2012) in Equation 1:

Equation 1. $J_w = \frac{\mathbb{P}}{l}(x_w \gamma_w P_w^{sat} - y_w P)$

Where:
J_w is water flux [kg m^{-2} h^{-1}]
$\mathbb{P}$ is the intrinsic membrane permeability [kg m m^{-2} h^{-1} bar^{-1}]
l is the membrane thickness [m]
x_w is the feed side liquid water mole fraction []
γ_w is the feed side water activity coefficient []
P_w^{sat} is the feed side water saturation pressure [bar]
y_w is the permeate side vapor phase water mole fraction []
P is the total permeate pressure [bar]

Since the feed side water saturation pressure is defined by the Antoine equation (describing an exponential relationship between saturation pressure and temperature), these processes can be described as either vapor pressure driven or temperature driven (Baker 2012).

Equation 1 describes a process where the permeate side is a vapor. For DCMD, Equation 1 is modified to include a second term containing the liquid phase water mole fraction, $x_w \gamma_w P_w^{sat}$, for the permeate side vapor pressure.

In theory, according to Equation 1, there is no high limit for the solute feed concentration. However, solubility limits can be exceeded causing scaling. Since the water mole fraction goes down as the solute mole fraction goes up, water flux will be lower at high solute feed concentrations.

While MD and pervaporation desalination are similar, there are important differences. In pervaporation, water evaporates through a dense hydrophilic membrane. Pervaporation membranes play an active role in separating water from salt. In MD, water evaporates though an openly porous hydrophobic membrane. Porous MD membranes serve as a contactor surface in which the phase change from liquid to vapor occurs and then vapor flows through the open porous structure. Membrane wetting and conductive heat loss through the membrane occur in MD—but not pervaporation desalination (Liang et al 2015). In addition, hydrophilic membranes used in pervaporation desalination are less prone to biofouling than the hydrophobic membranes used in MD.

1.2.2.3. State of the Art in Pervaporation for Desalination and Wastewater Recovery

In pervaporation, separations such as ethanol from water in biofuel production, two or more components pervaporate through the membrane. The mechanism by which sodium chloride (NaCl) appears in the permeate condensate is not known. Sodium chloride transport through a pervaporation membrane is probably by means of diffusion of bulky hydrated ions. This process is not described by Equation 1.

Table 2 presents a summary of reported desalination performance of pervaporation membranes. As seen in Table 2, many pervaporation membranes have very high salt rejection (>99%) and can extract water from very high salinity waters. It is well known that heating the feed water will result in an increase in water flux through a pervaporation membrane based on the driving for transport and the solution diffusion model of transport through these membranes (Feng and Huang 1996). For example, Zwijnenberg et al. (2005) described a solar driven membrane pervaporation process for desalination where the feed solution was heated by solar irradiation. However, for a given membrane, an increase in water flux will result in higher concentration polarization and an increase in the permeate solute concentration. Most of the studies shown in Table 2 are for low concentration NaCl feeds. Two studies (Naim et al. 2015 and Liang et al. 2015) used higher concentration feeds of the type that may represent RO concentrates. The graphene oxide membranes used by Liang et al. 2015 appear to show the best flux and separation. The Liang et al. (2015) study documents the effect of increasing feed solute concentration: as the feed concentration increased, the solute permeate concentration increased and the rejection and the water flux decreased. The effect on rejection of varying feed concentration was very small with all rejections >99.8%. At 35 g L^{-1} NaCl and 90 degrees Centigrade (°C), a water flux of 65.1 kilograms per meter squared hour (kg m^{-2} h^{-1}) and rejection > 99.8% were achieved. This result is competitive with anything achieved by MD. The studies represented in Table 2 use conventional (non-nanophotonic) membranes. The flux and separation performance of nanophotonic enhanced membranes are projected to be superior to those shown in Table 2.

Very limited research has investigated pervaporation as a high salinity and brine management technique (Shen and Lefebvre 1993, Sheng 1994, and Yacou et al. 2015). However, we argue that pervaporation is best suited to use with high salinity waters. Sheng and Lefebvre (1993) investigated the feasibility of proprietary hydrophilic hollow fiber membranes for pervaporative concentration of the brine stream from an osmotic distillation process. They studied brine streams with concentrations of 100 to 180 grams per liter (g/L) NaCl. As expected from pervaporation, their process had very high solute rejections. Their preliminary lab-scale results were promising and resulted in a pilot scale test Sheng (1994). In the pilot-scale experiment, pervaporation fluxes were slightly lower than in the lab scale.

Table 2.—Performance Summary of Hydrophilic Pervaporation Membranes Used for Desalination Reported in the Literature

Citation	Membrane type	Feed conc. NaCl (g L^{-1})	Feed temperature. $^\circ$C	Permeate flux kg m^{-2} h^{-1}	Salt rejection %	Water permeance *10^7 mol m^{-2} s^{-1} Pa^{-1}
Korngold et al. 1996	polyethylene ion exchange	NA	50	2.25	NA	13.8
Korin et al. 1996	sulfonated polyethylene	60	50	2	NA	32.3
Naim et al. 2015	Cellulose acetate-based	140	70	5.97	90	32.3
Chaudhri et al. 2015	polyvinyl alcohol (PVA)	30	70	7.4	99.9	39.8
Xie et al. 2011	PVA/maleic acid/silica hybrid	2	22	7	99.9	596
Swenson et al. 2011	natural clinoptilolite (zeolite)	0.1	93	2.5	97.5	4.9
Drobek et al. 2012	ZSM-5 (zeolite)	3	75	11.5	99	46.2
An et al. 2014	clinoptilolite phosphate	1.4	95	15	95	22.7
Liang et al. 2014	thin film nanofibrous PVA	50	25	5.81	99.8	299
Liang et al. 2015	graphene oxide polyacrylonitrile	100	30	11.23	99.8	423
Zhou et al. 2016	faujasite on alumina	35	90	5.64	99.8	12.5
Yacou et al. 2015	titanium dioxide on alumina	35	75	7	99	28

1.2.2.4. Nanophotonics and the Photothermal Effect

Researchers in the broad field of nanophotonics have previously established that nanoparticles of surface-plasmon-resonant noble metals, semiconductors, and carbon can exhibit photothermal effects (Fang et al. 2013, Govorov and Richardson 2007, and Lukianova-Hleb et al. 2010). Examples of nanophotonic materials are carbon black, silver nanoparticles, and gold nanoparticles. The photothermal effect occurs when materials are capable of directly converting light energy to thermal energy (e.g., the particles heat themselves and their surroundings). This photothermal effect has been extensively studied for and used in imaging, sensing, biology and medicine (Neumann et al. 2013). Much of the previous research on nanophotonic photothermal materials has focused on irradiating particles with very specific wavelengths of light (such as from a laser or light-emitting diode [LED]). Certain nanophotonic materials exhibiting the

photothermal effect are capable of high conversion of the entire solar spectrum into thermal energy, with efficiencies up to 80% (Jiang et al. 2013).

In pervaporation, flux enhancement by heating the feed (and the membrane) occurs both because of an increase in feed vapor pressure and dissipation of the concentration polarization layer at the feed/membrane interface. Therefore, nanophotonic heating of the membrane should result in membrane performance improvements (such a flux increases).

1.2.2.5. Previous Applications of Nanophotonics and the Photothermal Effect in Membrane Science

There is limited use of the photothermal effect in both membrane science and environmental engineering. In this section, we summarize the major research applying the photothermal effect of nanoparticles to four types of membrane separations.

Nanophotonic Enhanced Solvent Nanofiltration Membranes
Vanherck et al. (2011 [Localized Heating]) synthesized 5 to 20 nanometers (nm) of gold nanoparticles within cellulose acetate membranes for nanofiltration of alcohol and water solutions and measured the solvent flux through the membranes with and without irradiation of a continuous wave argon-ion laser beam (with a wavelength of 514 nm). They found that average permeance increased by 167% while the membranes were irradiated with the laser, while there was no statistically significant change in average rejection. Again, Vanherck et al. showed 50 to 400% flux improvements in gold (Au) nanoparticle and polyimide nanofiltration membranes when they were irradiated with argon-ion laser beams without significant change in solute rejection during alcohol/bromothymol blue filtrations Vanherck et al. (2011 [Photothermal]) In another case, Li et al. (2014) incorporated silver (Ag) nanoparticles into cellulose acetate membranes and irradiated them with LED light during solvent nanofiltration of Rose Bengal in water, isopropanol, and ethanol. They found that permeances increased more in the membranes with the silver (Ag) nanoparticles when illuminated with the LED than the ones without, while solute rejection did not change significantly. Depending on the synthesis method to incorporate nanoparticles into the membrane, Li et al. (2014) observed significant nanoparticle leaching from their membranes.

Nanophotonic Enhanced Pervaporation Membranes
Two reports discuss nanophotonic enhanced pervaporation membranes (Li et al. 2013 and Russell 2012). Li et al. (2013) incorporated 2 to 15 nm diameter Ag-nanoparticles *in situ* during the synthesis of polydimethylsiloxane (PDMS) membranes for pervaporation of ethanol from dilute aqueous solutions. Li et al. (2013) irradiated the membranes with LED light and found increases up to 100% in fluxes in the nanophotonic enhanced membrane while maintaining selectivity. They also found that the permeate sweep flow rate had an influence on performance, and that a sweep flow rate that was too high could be detrimental.

Russell (2012) reports illuminating gold nanoparticle/PDMS membranes with laser light significantly increased the temperature of the membrane as well as enhanced the flux up to 117% for butanol/water separations.

Nanophotonic Enhanced Pressure Driven Water-Filtration Membranes

Hu et al. (2015) synthesized Au nanorods/poly(N-isopropylacrylamideco - acrylamide) co-hybrid single-walled carbon nanotube (SWCNT) fibrous membranes and tested them for the filtration of a nano-emulsion of n-hexadecane in water. The Au nanorods exhibit the photothermal effect with up to 160% increases in permeate fluxes when illuminated with laser light.

Nanophotonic Enhanced Membrane Distillation Membranes

An investigation of nanophotonic enhanced direct contact membrane distillation (DCMD) for desalination incorporates nanophotonic carbon black particles onto the surface of a thin hydrophilic PVA layer which is coated onto a hydrophobic commercial poly vinylidene fluoride support (Dongare et al. 2017). Their experimental design minimized the contribution to flux by conventional MD (by using a small temperature difference between the water on the feed and permeate sides) and irradiative heating (minimizing the time that a given feed volume is exposed to light). They achieved a flux of 5.38 kg m^{-2} h^{-1} by the nanophotonic photothermal effect under 25x solar light exposure (Halas and Li 2015). Carbon black, silver, and gold nanoparticles achieve up to 80% conversion efficiency of light to thermal energy (Jiang et al. 2013).

Criscuoli et al. (2008) reported that vacuum membrane distillation had an energy consumption/permeate flow ratio about three times lower than DCMD measured in kilowatts per kilograms per hour (kW/kg h). The question can be asked: why not choose VMD over DCMD for nanophotonic enhancement? Ashoor et al. (2012) state in their comprehensive review of DCMD that "the direct control of permeate temperature is not possible in vacuum membrane distillation and a high pressure variation can occur on the membrane surface in vacuum membrane distillation which can result in wetting or reduction of hydrophobicity of the membrane. Therefore, most research on vacuum membrane distillation has focused on removing volatile organic compounds such as ethanol, with only minimal studies on desalination."

Heat flux across the membrane in direct contact membrane distillation, according to Alkhudhiri et al., (2012) is the sum of the conductive heat flux and the heat flux due to vaporization of the permeate. The first of these terms, the conductive heat flux, is the product of the membrane heat transfer coefficient and the transmembrane temperature differential. The second term is the product of the permeate flux and the latent heat of vaporization. In vacuum membrane distillation, heat transfer through the membrane is ignored, and is represented by the product of permeate flux and the latent heat of vaporization. According to Favre (2003), transmembrane heat flux in pervaporation is the same as transmembrane heat flux in vacuum membrane distillation (i.e. the product of permeate flux and the latent heat of vaporization. Eykens et al. (2016) reviewed MD configurations and stated that conductive heat loss is one of the main

disadvantages of DCMD. This conductive heat loss may account for the difference in the energy consumption and permeate flow rate between DCMD and VMD. It can be argued that because of the similarities of pervaporation desalination with VMD that the energy consumption and permeate flow rate ratios are similar. Additionally, in pervaporation desalination, controlling the temperature of the permeate is generally not a concern, nor is wetting or reducing the membrane's hydrophobicity. Pervaporation desalination thus has the advantage of requiring less energy per unit of flux than DCMD, but it does not have the disadvantages of VMD.

DCMD generally achieves higher fluxes than those obtained in pervaporation desalination. However, this conclusion may be premature as relatively few studies have reported on pervaporation desalination. Liang et al. (2015) reported an example of high flux achieved by pervaporation desalination. They recorded a flux of 65 kg m^{-2} h^{-1} using a graphene oxide membrane with a feed of 35 g/L NaCl at 90 °C. It is anticipated that continued research on pervaporation desalination membranes will show continued performance improvement. Additionally, the cost of pervaporation desalination is less than the cost of DCMD based on energy efficiency.

Flux of water (and solutes) in MD is described by the pore flow model. The driving force for separations with MD is the partial vapor pressure difference across the membrane (primarily driven by a temperature difference across the membrane). Therefore, the Nanotechnology Enabled Water Treatment (NEWT) Center is investigating the heating effect of nanophotonic materials to minimize thermal polarization at the surfaces of membrane distillation membranes (Li et al. 2016). A vapor pressure gradient across the membrane is the driving force in MD as well as in pervaporation desalination. Because vapor pressure increases exponentially with temperature, there is a sharp rise in flux as the feed temperature is increased. Pervaporative desalination is a low energy alternative for desalination, compared to membrane distillation, according to Bolto et al. (2010). It may be superior to MD as material costs and conductive heat loss from the feed to the permeate are reduced (Bolto et al. 2010).

1.3. Project Overview

We used mathematical analysis of the nanophotonic photothermal effect coupled with direct solar radiation to improve the performance of pervaporation membranes for high salinity water recovery. Nanophotonic flux enhancement may be better for pervaporation desalination than DCMD because pervaporation desalination does not have conductive heat loss through the membrane.

1.3.1. Overall Approach and Concepts

The overall approach was to:

1) Combine computational and experimental methods to evaluate hybrid processes for the treatment of inland brackish water desalination concentrate.

2) Develop novel nanophotonic enhanced pervaporation membranes. Figure 2 shows the overall hybrid desalination concept for which we calculated multi-stage RO followed by pervaporation.

3) Develop a method for coating nanophotonic particles onto commercially available pervaporation membranes.

4) Build a laboratory-scale cross-flow pervaporation system to evaluate the performance (flux, rejection, and recovery) of pervaporation and nanophotonic enhanced pervaporation processes.
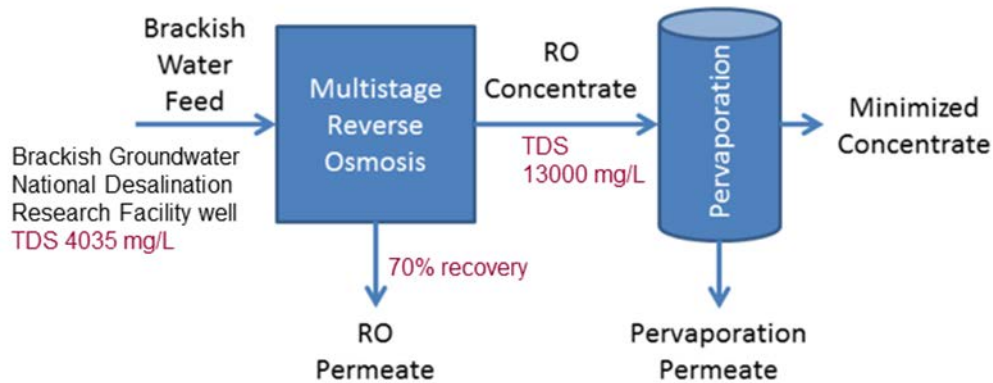
Figure 2.—Schematic of overall project concept for combined reverse osmosis and pervaporation system.

1.3.2. Overall Method

The method used for the first task mentioned in Section 1.3.1, computational modeling, was based on the RO process analysis described in Crittenden et al. 2012. The equations were put into an Excel program (a detailed explanation follows in the next section) and were modified as necessary for pervaporation. The program can be used to simulate RO, pervaporation desalination, or a combination of these. A variety of feed waters were run through the simulation, including NaCl 2 g/L BGNDRF, and Buckeye well waters. The RO simulations used the other process variable values from Crittenden et al. (2012) with the exception of running different initial hydraulic pressures (Table 3 and Table 4). A

variety of different values for process inputs were used for the pervaporation portion including different feed temperatures, water mass transfer coefficients, and Reynolds exponents for the Sherwood correlations. A chief objective of the modeling was to show the extent of concentration polarization in RO and pervaporation. A large amount of concentration polarization can lead to impaired water flux and can increase the propensity for scaling when the feed contains sparingly soluble salts (e.g., calcium salts).

The methodology for the second task mentioned in Section 1.3.1, the development of novel nanophotonic pervaporation membranes was to paint carbon black onto commercial pervaporation membranes designed for organic dehydration. The membranes were asymmetric PVA membranes supplied by DeltaMem. These first generation nanophotonic membranes were tested for efficacy by running pervaporation studies on the virgin membranes with and without exposure to a Xenon lamp (solar simulator) and comparing the results to pervaporation studies using the carbon black coated membranes with and without exposure to a Xenon lamp.

A link between the two tasks was found by means of theoretical analysis. Concentration polarization mitigation occurs as a consequence of nanophotonic heating of pervaporation membranes. A detailed analysis of concentration polarization and concentration polarization mitigation in pervaporation desalination is presented in Section 2. Technical Approach and Methods.

2. Technical Approach and Methods:

2.1. Methodology for Excel Modeling of Concentration Polarization in RO and Pervaporation

Calculations and experiments were performed at Arizona State University and the University of Texas at El Paso, using Excel for modeling. The modeling methodology for the Excel program was obtained from Crittenden et al. (2012).

The model used for concentration polarization in RO and pervaporation is taken from Crittenden et al. (2012) and built into an Excel program (Crittenden et al. [2012]'s RO model was modified for pervaporation). The figure represents the physical aspects of the RO portion of the model. The pervaporation portion of the model is similar to the RO portion, the exception is the calculation of solute permeate concentration. In RO solutes, permeate concentration decreases with increasing water flux. In pervaporation solutes, permeate concentration increases with increasing water flux. The first set of equations are for the RO portion of the model. The modification for the solute permeate concentration calculation is described below.
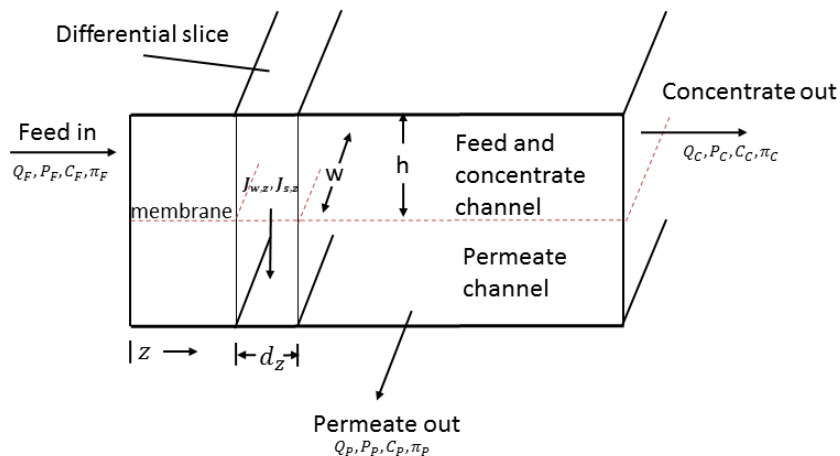
Figure 3.—Process variables in one increment of RO model inspired by Crittenden et al. (2012).

These steps are required for the iterative calculations per increment to obtain recovery and rejection per increment, per element, per stage, and per process. In Figure 3, showing the process variable of one increment in the model, dz represents one increment (0.1 meter [m]). Figure 4, Figure 5, and Figure 6 show a

top-down illustration of the model. In Figure 6, increment 1, etc. is the same as dz in Figure 3.
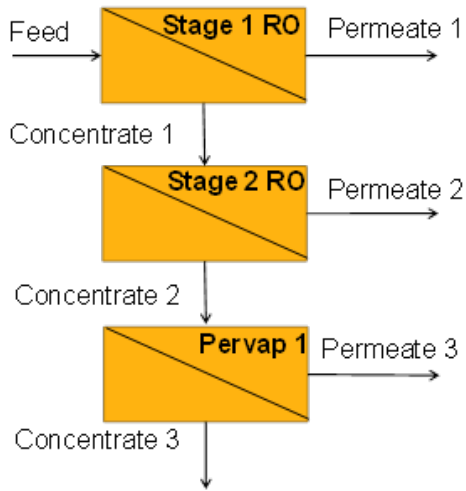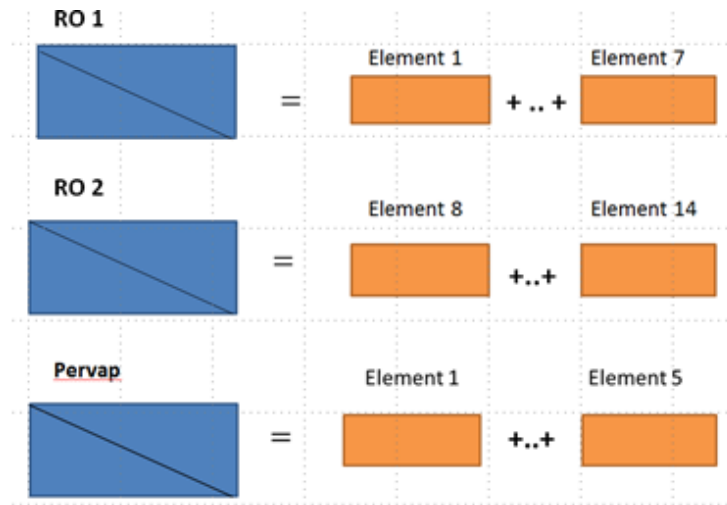

Figure 4.—RO and pervaporation stages.

Figure 5.—Each RO stage contains seven elements; each pervaporation stage has 5 elements.
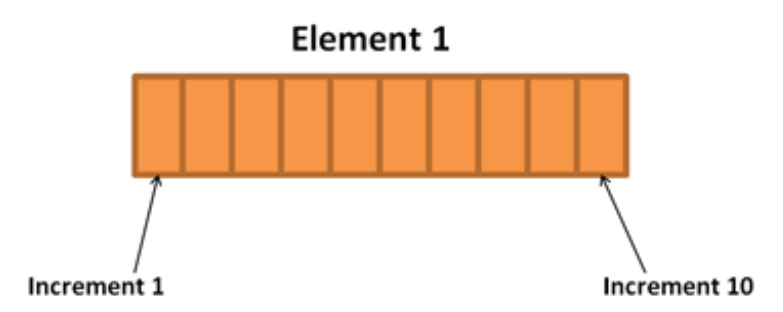

Figure 6.—Each element is divided into ten increments.

The calculations make use of the values in Table 3, Table 4, Table 5, and Table 6.

Table 3.—Initial Values for RO Model (Crittenden et al. 2012)

Parameter	Units	Value
Feed flow	$m^3 s^{-1}$	$3.125*10^{-3}$
Feed Pressure (P_F)	bar	14.2
Feed Concentration	$mg\ L^{-1}$ NaCl	2000
Permeate Pressure	bar	0.3
Head loss coefficient	$bar\ s^2\ m^{-3}$	0.8

Table 4.—Membrane Properties (Crittenden et al. 2012)

Membrane properties	Units	Value
Water mass transfer coefficient (k_w)	$L\ m^{-2}\ h^{-1}\ bar^{-1}$	2.87
Solute (NaCl) mass transfer coefficient	$m\ h^{-1}$	$6.14*10^{-4}$
Diffusion coefficient NaCl (D_{NaCl}) – boundary layer	$m^2\ s^{-1}$	$1.35*10^{-9}$

Table 5.—Summary of Water Quality Data

Parameter	Units	BGNDRF	BGNDRF 70% concentrate	Buckeye
TDS	mg/L	4035	13450	1583
$CaCl_2$	mg/L	1220	4067	262
Na_2SO_4	mg/L	1350	4500	176
$MgSO_4$	mg/L	1090	3633	120
$NaHCO_3$	mg/L	340	1133	142
NaCl	mg/L	0	0	883
Sodium Silicate	mg/L	35	117	0

Table 6.—Process Variables for RO and Pervaporation Models

Input	Semi-fixed	Output
Feed volumetric flow rate	# elements per stage	Permeate flow rate
Feed concentration	Element length	Permeate solute concentrate
Feed hydraulic pressure (RO only)	# of increments per element	
Feed temperature	Feed channel width	
	Feed channel height	
	Feed channel head loss (RO)	
	Water mass transfer coefficient	
	Solute mass transfer coefficient	
	Diffusion coefficient NaCl	
	Reynolds number exponent	

2.1.1. Step 1. Calculate the Solute Boundary Layer Mass Transfer Coefficient

Calculating the solute boundary layer mass transfer coefficient, k_{cp} [m s^{-1}], is done by using a Sherwood correlation, Sh, (Equation 6). First calculate the feed velocity using Equation 2:

Equation 2. $v_z = \frac{Q_F}{hw}$

Where:
v_z is the feed channel velocity [m s^{-1}]
Q_F is the feed volumetric flow [m^3 s^{-1}]
h [m] is the feed channel height
w [m] is the feed channel width

Then obtain the hydraulic diameter using Equation 3 through Equation 6:

Equation 3. $d_H = 2h$

Where:
d_H [m] is the hydraulic diameter
h [m] is the feed channel height

Equation 4. $Re = \frac{\rho v_z d_H}{\mu}$

Where:
Re is the Reynolds number [ ]
ρ is the water density [kg m^{-3}]
μ is the water viscosity [kg m^{-1} s^{-1}]
v (v$_z$) is the feed channel velocity [m s^{-1}]
d$_H$ [m] is the hydraulic diameter

Equation 5. $Sc = \frac{\mu}{\rho D_{NaCl}}$

Where:
Sc is the Schmidt number [ ]
ρ is the water density [kg m^{-3}]
μ is the water viscosity [kg m^{-1} s^{-1}]
D$_{NaCl}$ is the solute diffusion coefficient [m^2 s^{-1}]

Equation 6. $k_{cp} = 0.023 \left(\frac{D_{NaCl}}{d_H}\right) Re^{0.83} Sc^{0.33}$

Where:
D$_{NaCl}$ is the solute diffusion coefficient [m^2 s^{-1}]
d$_H$ [m]is the hydraulic diameter
Re is the Reynolds number [ ]
Sc is the Schmidt number [ ]
k_{cp} is the solute boundary layer mass transfer coefficient [m s^{-1}]

Equation 6 shows a Reynolds number of 0.83 for RO as obtained from Crittenden (2012). For pervaporation desalination, a Reynolds number of 0.3 was found to correlate with the experimental data obtained from literature analysis.

2.1.2. Step 2. Calculate the Feed Osmotic Pressure

Calculate the feed osmotic pressure using Equation 7:

Equation 7. $\pi = CRT$

Where:
π is the osmotic pressure [bar]
C is the ion concentration [mol L^{-1}]
R is the gas constant [L bar mol^{-1} K^{-1}]
T is the temperature [K]

2.1.3. Step 3. Calculate Water Flux and Concentration Polarization Modulus for the First Increment

Equation 8 and Equation 9 are solved simultaneously to obtain the concentration polarization modulus C_z' and the incremental water flux $J_{w,z}$. Assume rejection=1 for first increment.

Equation 8. $C_z' = exp\left(\frac{J_{w,z}}{k_{cp}}\right) * Rej + (1 - Rej)$

Where:
C_z' is the concentration polarization modulus [ ] in increment z
k_{cp} is the solute boundary layer mass transfer coefficient [m s^{-1}]
$J_{w,z}$ is the incremental water flux [L m^{-2} h^{-1}]
Rej is rejection [ ]

Equation 9. $J_{w,z} = k_w[(P_F - P_P) - (C_z'\pi_F - \pi_P)]$

Where:
$J_{w,z}$ is the incremental water flux [L m^{-2} h^{-1}]
k_w is the membrane water mass transfer coefficient (an assumed constant) [L m^{-2} h^{-1} bar^{-1}]
P_F is the hydraulic feed pressure [bar]
P_P is the hydraulic permeate pressure [bar]
C_z' is the concentration polarization modulus [ ]
π_F is the feed osmotic pressure [bar]
π_P is the permeate osmotic pressure [bar].

2.1.4. Step 4. Calculate the Solute Flux and Solute Transport Across the Membrane

Equation 10 and Equation 11 are used to calculate the solute flux and solute transport across the membrane. See Crittenden et al. 2012, Chapter 17 Section 7 for a detailed explanation.

Equation 10. $J_{s,z} = k_s C_z' C_F - C_P)$

Where:
$J_{s,z}$ is the solute flux [mg m^{-2} h^{-1}]
k_s is the solute membrane mass transfer coefficient [m h^{-1}]
C_z' is the concentration polarization modulus [ ]
C_F is the solute feed concentration [mg m^{-3}]
C_F is the solute feed concentration[mg m^{-3}]

Equation 11. $M_{s,z} = J_{s,z}(w)(dz)$

Where:
$M_{s,z}$ is the solute transmembrane mass transfer rate [mg s^{-1}]
$J_{s,z}$ is the solute flux [mg m^{-2} h^{-1}]
w is the feed channel width [m]
dz is the feed channel incremental length [0.1 m]

2.1.5. Step 5. Calculate the Permeate Flow Rate

Use Equation 12 to calculate the permeate flow rate:

Equation 12. $Q_P = J_{w,z}(w)(dz)$

Where:
Q_P is the permeate flow rate [m^3 s^{-1}]
$J_{w,z}$ is the incremental water flux [L m^{-2} h^{-1}]
w is the feed channel width [m]
dz is the feed channel increment length [0.1 m]

2.1.6. Step 6. Calculate the Inputs for the Second and Subsequent Increments

The second and subsequent increments are calculated using the output from the previous increment. In increments following the first increment the permeate concentration is not zero. Calculate the feed volumetric flow and velocity using Equation 13 and Equation 14.

Equation 13. $Q_{F2} = Q_F - Q_P$

Where:
Q_{F2} is the feed volumetric flow in the second increment [m^3 s^{-1}]
Q_F is the feed volumetric flow rate for the first increment [m^3 s^{-1}]
Q_P is the permeate flow rate for the first increment [m^3 s^{-1}]

Equation 14. $v_{z2} = \frac{Q_{F2}}{hw}$

Where:
v_{z2} is the feed velocity in the second increment [m s^{-1}]
Q_{F2} is the feed volumetric flow in the second increment [m^3 s^{-1}]
h is the feed channel height [m]
w is the feed channel width [m]

Use Equation 15 to calculate the feed concentration for the second increment:

Equation 15. $C_{F2} = \frac{Q_F C_F - M_{s,z}}{Q_{F2}}$

Where:
C_{F2} is the feed concentration in the second increment [mg L^{-1}]
Q_F is the feed volumetric flow rate in the first increment [m^3 s^{-1}]
C_F is the feed concentration in the first increment, [mg L^{-1}]
$M_{s,z}$ is the solute transmembrane mass transfer rate [mg s^{-1}]
Q_{F2} is the feed volumetric flow in the second increment [m^3 s^{-1}]

Use Equation 16 to calculate the permeate concentration for the second increment.

Equation 16. $C_{P2} = \frac{J_{s,z}}{J_{w,z}}$

Where:
C_{P2} is the solute concentration in the second increment permeate [mg L^{-1}]
$J_{s,z}$ is the solute flux [mg m^{-2} h^{-1}]
$J_{w,z}$ is the incremental water flux [L m^{-2} h^{-1}]

Use Equation 17 to calculate the head loss for the second increment.

Equation 17. $h_{L2} = \delta_{HL}(v_z)^2 dz$

Where:
h_{L2} is the head loss in the second increment [bar]
δ_{HL} is the head loss coefficient [bar s^2 m^{-3}]
v_z is the feed velocity in the first increment
dz is the feed channel incremental length [0.1 m]

Use Equation 18 to calculate the feed pressure in the second increment.

Equation 18. $P_{F2} = P_{F1} - h_{L2}$

Where:
P_{F2} is the feed pressure in the second increment [bar]
P_{F1} is the feed pressure in the first increment [bar]
h_{L2} is the head loss in the second increment [bar].

Use Equation 19 to calculate the osmotic pressure of the permeate in the second increment.

Equation 19. $\pi = C_{P2}RT$

Where:
π is the osmotic pressure of second increment permeate [bar]
C_{P2} is the solute ion concentration in the second increment permeate [mol L^{-1}]
R is the gas constant [L bar mol^{-1} K^{-1}]
T is the temperature [K].

Use Equation 20 to calculate the osmotic pressure of the feed in the second increment.

Equation 20. $\pi = C_{F2}RT$

Where:
π is the osmotic pressure of the second increment feed
C_{F2} is the ion concentration of the second increment feed [mol ion L^{-1}]
R is the gas constant [L bar mol^{-1} K^{-1}]
T is the temperature [K]

Repeat steps 1-6 for each RO increment.

When there is a stage change, the permeate concentration of the first increment of the new stage is zero.

2.1.7. Calculate Flux and Rejection

We modified the pervaporation portion of the model to include the inverse relationship between flux (recovery) and rejection found by applying the thin film boundary layer theory to published pervaporation desalination data as shown in Equation 21 (Table 7).

Equation 21. $c_{ip,z} = \dfrac{c_{ib}}{\dfrac{\frac{1}{E_0}-1}{exp\left(\frac{v'\delta}{D_i}\right)}+1}$

Where:
$c_{ip,z}$ is the incremental solute permeate concentration [mg L^{-1}]
E_0 is the intrinsic enrichment []
c_{ib} is the bulk solute feed concentration [mg L^{-1}]
v' is the incremental volumetric water flux [m s^{-1}]
D_i/δ is the solute boundary layer mass transfer coefficient, obtained by a Sherwood correlation [m s^{-1}]
D_i is the solute (e.g. sodium chloride) diffusion coefficient [m^2 s^{-1}]
δ is the thickness of the boundary layer at the feed/membrane interface [m]
Equation 21 is Equation 45 (defined below) rearranged.

The pervaporation portion of the model uses Equation 1 for water flux. In

Equation 1, P_w^{sat} is obtained from the inputted temperature from the Antoine equation. Two simplifying assumptions are made:

1) Use zero as the permeate pressure because a vacuum exists on the permeate side in pervaporation.

2) Use a water activity coefficient (γ_w) of 1. This assumption is valid up to about 3M NaCl and covers most of the feed concentrations obtained or used in the model (Miyawaki et al. 1997).

Additionally, hydraulic and osmotic pressures were not used for the pervaporation portion of the model.

The differences between the RO and pervaporation portion are:

1) Hydraulic and osmotic pressure differences do not drive flux in pervaporation (not an input to the pervaporation model) – pervaporation operates without a hydraulic pressure head

2) The solute permeate concentration decreases with increasing water flux in RO and increases with increasing water flux in pervaporation

The RO solute permeate concentration is a simple function using a constant solute mass transfer coefficient (Equation 1) whereas in pervaporation desalination, the solute permeate concentration is a more complicated function of the solute bulk feed concentration, intrinsic enrichment and the Peclet number $(\frac{v'\delta}{D_i})$ (dimensionless). The Peclet (pronounced "Pe-CLAY") number is named after a 19th century French engineer who worked on the ventilation systems of a number of Parisian buildings (Nicholls 1922). The original definition of the Peclet number is the ratio of the convective heat flow to the conductive heat flow (Nieto et al. 2014). Subsequently, the definition was modified for mass transport to Equation 1. The Peclet number has a wide variety of applications beyond that of membrane science (Huysmans and Dassargues 2005).

To obtain the total solute permeate concentration in RO, use Equation 22:

Equation 22. $c_{ip} = \frac{\Sigma J_{i,z}}{\Sigma J_{w,z}}$

Where:
c_{ip} is the total solute permeate concentration [mg L^{-1}].

To obtain the total solute permeate concentration in pervaporation, use Equation 23:

Equation 23. $c_{ip} = \frac{\sum c_{ip,z} Q_{p,z}}{\sum Q_{p,z}}$

Where:

$Q_{p,z}$ is the incremental permeate volumetric flow rate [L s^{-1}]

$c_{ip,z}$ is obtained from Equation 21

There is a major difference in the results obtained from Equation 22 and Equation 23. In RO, total solute permeate concentration decreases with increased water flux. In pervaporation, total solute permeate concentration increases with increased water flux.

2.2. Concentration Polarization Theory and the Theory of Concentration Polarization Mitigation with Nanophotonic Pervaporation Membranes

Equations for Sections 2.2 through 2.8:

Equation 24. $Pe = \frac{solute\ convective\ velocity}{solute\ diffusive\ velocity}$

Equation 25. $Pe = \frac{v'\delta}{D_i}$

Equation 26. $C' = \exp\left(\frac{v'\delta}{D_i}\right)$

Equation 27. $C' = \frac{c_{i0}}{c_{ib}}$

Equation 28. $C' = \exp(Pe)$

Equation 29. $v'c_{ip} = v'c_i - D_i\frac{dc_i}{dx}$

Equation 30. $\frac{c_{i0} - c_{ip}}{c_{ib} - c_{ip}} = \exp\left(\frac{v'\delta}{D_i}\right)$

Equation 31. $\frac{D_i}{\delta} = \frac{J}{c_{ib} - c_{i0}}$

Equation 32. $v'c_i = D_i\frac{dc_i}{dx}$

Equation 33. $k_{SH} = \frac{D_i}{\delta}$

Equation 34. $Sh = (constant)Re^\alpha Sc^\beta$

Equation 35. $Sh = \frac{k_{SH}d_h}{D_i}$

Equation 36. $\frac{k_{SH}d_h}{D_i} = (constant)Re^\alpha Sc^\beta$

Equation 37. $"V" = -\Delta P_{i,layer}$

Equation 38. $"V" = -\Delta\mu_{i,layer}$

Equation 39. $"V" = -\Delta c_{i,layer}$

Equation 40. $"I" = J_i$

Equation 41. $"R" = \frac{1}{F_{i,layer}}$

Equation 42. $\frac{1}{F_{i,total}} = \frac{1}{F_{i,boudary\ layer}} + \frac{1}{F_{i,membrane}}$

Equation 43. $k_0 = \frac{J_i}{(c_{ib} - c_{i0})}\left(\frac{m}{s}\right)$

$k_0 = RIS\ boundary\ layer\ mass\ transfer\ coefficient\ as\ \left(\frac{m}{s}\right)\left(\frac{D_i}{\delta}\right)$

Equation 44. $\frac{1}{F_{i,total}} = \frac{1}{k_0} + \frac{l}{Q_{i,int}}$

Equation 45. $\ln\left(\frac{1}{E} - 1\right) = \ln\left(\frac{1}{E_0} - 1\right) - \left(\frac{v'\delta}{D_i}\right)$

Equation 46. $E = \frac{c_{ip}}{c_{ib}}$

Equation 47. $E_0 = \frac{c_{ip}}{c_{i0}}$

Equation 48. $\lim\limits_{\delta \to 0} E = E_0$

$E = Enrichment$

$E_0 = intrinsic\ Enrichment$

Equation 49. $J_w = J_0 \exp\left(\frac{-E_a}{RT}\right)$

Equation 50. $J = J_0 \exp\left(\frac{-E_A}{R\left(T_b - \frac{\varphi}{h_0 + a\omega^\gamma}\right)}\right)$

Equation 51. $\varphi = J\Delta H_v$

Equation 52. $T_m = T_b - \frac{\varphi}{h_0 + a\omega^\gamma}$

Equation 53. $TPC = \frac{T_m - T_p}{T_b - T_p}$

Equation 54. $Q = h_0(T_b - T_m) = J\Delta H_v = \mathbb{P}_m(p_m - p_p)\Delta H_v$

Equation 55. $q_r + q_p = q_v + \left(q_{f,out} - q_{f,in}\right)$

Equation 56. $h_0(T_b - T_m) + q_p = J_w\Delta H_v$

Equation 57. $\Delta H = 4.1813\ \frac{J}{gK} * 1°K * 40.5\ g$

Equation 58. $m = \frac{Q}{C_p\Delta T}$

Concentration polarization is the phenomenon of higher or lower solute concentration, depending on the separation, in the feed side boundary layer relative to the bulk. According to Baker (2012), the boundary layer can be estimated to be about 20 micrometers (μm) thick. Ideally, the solute concentration in the boundary layer would be directly measurable. However, this type of measurement is not practical as the layer is only micrometers thick, which makes using a conductivity probe difficult. This is evidenced by the absence of research reporting on these measurements well as the abundance of research describing various ways of indirectly obtaining this concentration. The indirect approach for determining the solute concentration in the boundary layer uses a theoretical model, often incorporating experimental data.

Many studies of transport in the feed side boundary layer use the dimensionless Peclet number to help to describe the concentration polarization effect. The Peclet number (Pe) can be generally defined by Equation 24. Note, all equations in this section describe mass transport in the boundary layer (Bhattacharya and Hwang 1997 and Baker 2012).

Equation 24. $\text{Pe} = \frac{solute\ convective\ velocity}{solute\ diffusive\ velocity}$

A determination can be made, based on the solute profile in the boundary layer, as to whether the solute convective velocity is larger or smaller than the solute diffusive velocity (i.e. whether the Peclet number is larger or smaller than 1). Equation 24 should not be ignored because it places a mathematical constraint on TFBLT (see Equation 9). Alternatively, in the concentration polarization literature, the Peclet number is defined by Equation 25 (Bhattacharya and Hwang 1997):

Equation 25. $\text{Pe} = \frac{v'\delta}{D_i}$

Where:
Pe is the Peclet number [-]
v' is the volumetric water flux [$m^3\,m^{-2}\,s^{-1}$, or $m\,s^{-1}$]
δ is the boundary layer thickness [m]
D_i is the solute mass diffusion coefficient [$m^2\,s^{-1}$]

The Peclet number is dimensionless. The numerator is v' [$m\,s^{-1}$], volumetric water flux, and the denominator is $\frac{D_i}{\delta}$ [$m\,s^{-1}$].

The volumetric water flux, v' [$m\,s^{-1}$], is easily measured. The denominator of the Peclet number, $\frac{D_i}{\delta}$ [$m\,s^{-1}$], can be evaluated using one or more of several different models. The Resistance-in-Series (RIS) model, the method in Baker (2012) (a derivative of the thin film boundary layer theory [TFBLT]), and Sherwood correlations will be described.

In the RIS model:

$\frac{D_i}{\delta}$ is solute boundary layer permeance obtained by dividing solute molar flux, J [$mol\,m^{-2}\,s^{-1}$], by the boundary layer concentration differential [$mol\,m^{-3}$].

In the Sherwood correlations and Baker's method:

$\frac{D_i}{\delta}$ [$m\,s^{-1}$] is defined by dividing the solute diffusion coefficient D_i [$m^2\,s^{-1}$], by the boundary layer thickness, δ [m]. The ratio $\frac{D_i}{\delta}$ [$m\,s^{-1}$] is the solute boundary layer mass transfer coefficient (SBLMTC).

Once the volumetric water flux, v', and the SBLMTC are determined then the concentration polarization modulus, C' [-], can be determined using Equation 26:

Equation 26. $C' = \exp\left(\frac{v'\delta}{D_i}\right)$

Where:
C' is the concentration polarization modulus [-]
c_{i0} is the concentration of species i at the feed membrane interface [mol m^{-3}]
 c_{ib} is the bulk feed concentration of species i [mol m^{-3}]

The concentration polarization modulus is important because it provides a measure of flux impairment due to solute buildup in the boundary layer and provides for an assessment of the risk of scaling from sparingly soluble inorganic compounds present in the feed.

The concentration polarization modulus is defined by Equation 27.

Equation 27. $C' = \frac{c_{i0}}{c_{ib}}$

If Equation 24 is to be equated to Equation 25, one required approximation is the equating of solute convective velocity to the volumetric water flux, v'. Water flux is used as a convenient approximation for solute convective velocity in membrane desalination and volatile organic compounds (VOC) separation. If this assumption is made, then correspondingly the denominator in Equation 24, the solute diffusive flux, is equated to the denominator of Equation 25, the SBLMTC, $\frac{D_i}{\delta}$. If Equation 25 is substituted into Equation 26, Equation 28 is obtained:

Equation 28. $C' = \exp(Pe)$

Equation 26 is derived from the thin film boundary layer theory (TFBLT). There is no requirement, based on the TFBLT to use Equation 25 (i.e., to call the fraction appearing on the right hand side (RHS) of Equation 26 a Peclet number) although this is what is generally done in the literature. However, if Equation 28 is used to evaluate the concentration polarization modulus, C', then the Peclet number that results from Equation 24 should be consistent with that obtained from Equation 25. If, for example, Equation 24 suggests a Peclet number greater than one, than that is what should also be obtained by using Equation 25.

2.3. Thin Film Boundary Layer Theory and the Peclet Number

TFBLT is the underlying theory for evaluating concentration polarization, because Equation 26 results from it. The TFBLT postulates turbulent flow in the bulk feed transversely across a membrane. A layer of laminar flow exists between the bulk feed and the membrane. This layer is regarded as stagnant, with mass transport occurring only in a direction perpendicular to the membrane. The thin film boundary layer theory, as described by Brian (1966), and as discussed by Baker (2012) is based on the steady state Equation 29:

Equation 29. $v' c_{ip} = v' c_i - D_i \frac{dc_i}{dx}$

Where:

c_{ip} is the permeate concentration of species i [mol m^{-3}]

c_i is the concentration of species i in the boundary layer [mol m^{-3}]

x is the length dimension normal to membrane at the boundary layer [m]

The left-hand side (LHS) of Equation 29 represents the total flux of the solute. The first term on the RHS of Equation 29 represents the solute convective flux in the boundary layer, and the second term is the solute diffusive flux in the boundary layer. After separating variables and integration, Equation 30 is obtained:

Equation 30. $\frac{c_{io} - c_{ip}}{c_{ib} - c_{ip}} = \exp\left(\frac{v' \delta}{D_i}\right)$

For calculating the concentration polarization modulus, C' [-], Equation 30 is usually modified by assuming that the solute permeate concentration, c_{ip}, is zero. When the assumption of zero solute permeate concentration is made, Equation 26 results.

The Peclet number is represented in two ways in the TFBLT equations. The terms for the Peclet number, Equation 24 and Equation 25 can be found in the TFBLT equations, Equation 29 and Equation 30. This is illustrated by the red arrows showing interactions between these equations in Figure 7.
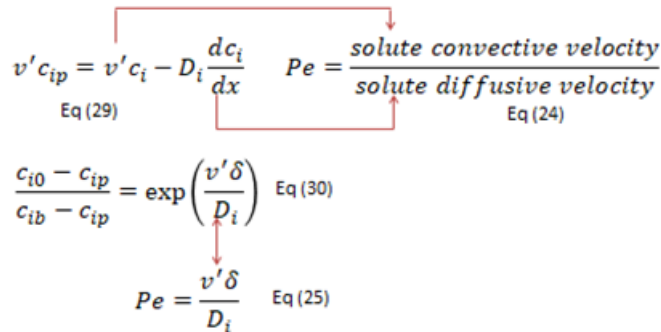

Figure 7.—Two definitions of Peclet number, Equation 24 and Equation 25, in TFBLT Equation 29 and Equation 30.

A modified version of Equation 30, Equation 35, was used to obtain the SBLMTC and the Peclet number in pervaporation desalination. First, the method of obtaining the SBLMTC and Peclet number in VOC separation from water is discussed.

Figure 8 illustrates the steady state solute concentration profile in the boundary layer in the case of VOC separation from water. This separation increases the VOC concentration in the liquid permeate relative to the bulk feed. As a consequence, at steady state, VOC concentration in the boundary layer is depleted. Convective solute (VOC) flux and diffusive solute flux in the boundary layer are towards the membrane resulting in positive permeate flux. VOC transport in the boundary layer is dominated by diffusion (Wijmans et al. 1995). When Equation 24 is used to assess the Peclet number, the Peclet number should be less than one for this separation.
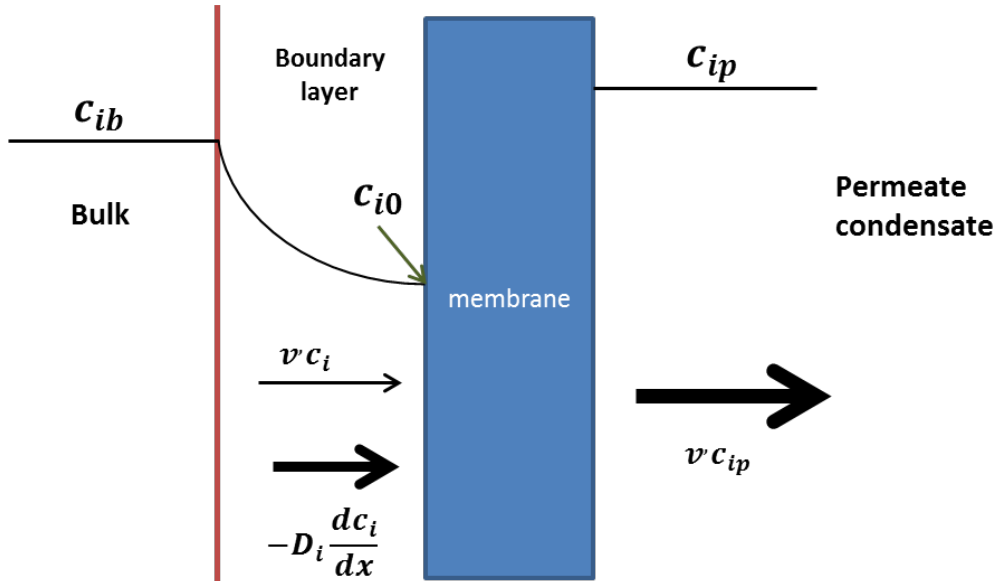
Figure 8.—Pervaporation VOC separation from water. Solute concentrations in the bulk feed, boundary layer, and permeate condensate. Relative contributions of convective and diffusive solute flux in the boundary layer to permeate flux.

If the convective term in Equation 29 is assumed to be zero (i.e., the diffusive VOC flux is much greater than convective VOC flux in the boundary layer), then Equation 31 is obtained:

Equation 31. $\frac{D_i}{\delta} = \frac{J}{c_{ib} - c_{i0}}$

Where:
J is VOC flux [mol m^{-2} s^{-1}]
$\frac{D_i}{\delta}$ [m s^{-1}]

The SBLMTC defined by Equation 31 is equivalently defined by the resistance in series (RIS) model. If the convective term in Equation 29 is assumed to be zero (i.e. the diffusive VOC flux is much greater than convective VOC flux in the boundary layer), then Equation 31 and Equation 32 are obtained.

2.4. Sherwood Correlations

When Brian (1966) discussed the TFBLT to evaluate concentration polarization in reverse osmosis, he used the Chilton-Colburn analogy to obtain the SBLMTC. The Chilton-Colburn analogy is similar to a Sherwood correlation. The Sherwood SBLMTC, k_{SH}, [m s^{-1}] is defined by Equation 33. According to a review by Gegas and Hallström (1987), the Sherwood correlation has the general form of Equation 34. The Sherwood number in Equation 34 is defined by Equation 35. Combining Equation 34 and Equation 35 results in Equation 36.

Equation 36. $\frac{k_{SH}d_h}{D_i} = (\text{constant})Re^\alpha Sc^\beta$

Where:
Sh is the Sherwood number [-]
Re is the Reynolds number [-]
Sc is the Schmidt number [-]
α, β are empirical exponents [-]
d_H is the hydraulic diameter [m]

Equation 36 allows for the determination of the boundary layer thickness, δ, if the diffusion coefficient and the bulk feed properties necessary for the determination of the Reynolds and Schmidt numbers are known. k_{SH} is equivalent to the SBLMTC, $\frac{D_i}{\delta}$ [m s^{-1}] and can be used in Equation 26 to obtain the concentration polarization modulus.

There are a number of caveats to using Sherwood correlations; the reader is referred to Gekas and Hallström (1987) review for a complete discussion of these caveats. They observe that the density and viscosity of the fluid changes in the boundary layer makes predictions based on bulk fluid properties less accurate. Also, Sherwood correlations do not commonly take the roughness of the membrane surface, membrane pores, etc. into account.

2.5. Resistance in Series

The resistance in series (RIS) model is the method for determining D_i/δ in VOC separation from water (Côté and Lipski 1988, Feng and Huang 1994, Bhattacharya and Hwang 1997, She and Hwang 2004, She and Hwang 2005, Fouad and Feng 2008, and Baker 2012). There are two parts to the resistance in series model. First Ohm's law is used (Equation 41). In Ohm's law, R is the resistance [ohms], V is the driving force [volts], and I is the current [amperes].

In membrane applications, the driving force, "V" can be defined in terms of the partial pressure difference between two layers, $\Delta P_{i,layer}$, (in kilopascals [kPa]), or the chemical potential difference between two layers for species i $\Delta\mu_{i,layer}$, [J mol^{-1}], or the difference in concentration of species i between two layers,

$\Delta c_{i,layer}$, [mol m^{-3}], Equation 37, Equation 38, and Equation 39. Figure 9 shows the concentration profile that has to exist for the RIS model to be applied.
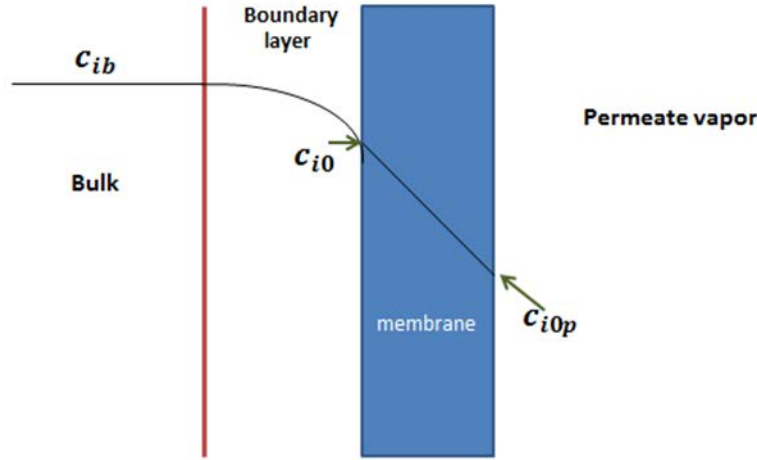
Figure 9.—Pervaporation separation of VOC from water, VOC concentration profile

The "current" can be defined as J_i the molar flux of species i [mol m^{-2} s^{-1}] (Equation 40).Therefore the resistance can be obtained as the reciprocal of the permeance of the species i of a layer, $F_{i,layer}$, in [mol m^{-2} s^{-1} kPa^{-1}], or [mol^2 m^{-2} s^{-1} J^{-1}], or [m s^{-1}], Equation 41. Secondly, the RIS model states that the total resistance is the sum of the individual resistances. The result is Equation 42.

Equation 42. $\dfrac{1}{F_{i,total}} = \dfrac{1}{F_{i,boudary\ layer}} + \dfrac{1}{F_{i,membrane}}$

The solute permeance of the boundary layer, $F_{i,boundary\ layer}$, is the SBLMTC, $\dfrac{D_i}{\delta}$ [m s^{-1}]. In the RIS model, the SBLMTC, $\dfrac{D_i}{\delta}$, is designated as k_0, [m s^{-1}] and is defined by Equation 43. The RHS of Equation 43 is identical to the RHS of Equation 31. It is therefore logical to conclude that $k_0 \left(\dfrac{D_i}{\delta} \right)$ is equivalent to the solute diffusive velocity, the denominator of Equation 24, because of the underlying assumption of zero convective velocity used for Equation 31.

This formulation of the RIS SBLMTC allows for comparison with the Sherwood SBLMTC, k_{SH}. k_0 can be obtained experimentally by evaluating Equation 44 (Côté and Lipski 1988, Fouad and Feng 2008):

Equation 44. $\dfrac{1}{F_{i,total}} = \dfrac{1}{k_0} + \dfrac{l}{Q_{i,int}}$

Where:
$F_{i,total}$ is the total permeance of species i [m s^{-1}]
l is the membrane thickness [m]
$Q_{i,int}$ is the intrinsic membrane permeability of species i [m^2 s^{-1}]

The total permeance is determined as a function of membrane thickness. Then a plot of Equation 44 gives $\frac{1}{k_0}$ as the intercept and $\frac{1}{Q_{i,int}}$ as the slope. Once k_0 $(\frac{D_i}{\delta})$ is known, then the concentration polarization modulus can be determined using Equation 26.

The resulting $\frac{v'\delta}{D_i}$ values that have been obtained, as reported in the literature, either with k_0, the SBLMTC obtained by the RIS model approach, or with k_{SH}, the SBLMTC obtained by a Sherwood correlation, are less than one. This is the same result as predicted by Equation 24.

2.6. Thin Film Boundary Layer Theory to Determine the SBLMTC and Peclet Number

Figure 10 illustrates the solute boundary layer concentration profile for membrane desalination. At steady state, the liquid permeate solute (e.g., NaCl) concentration is less than the solute concentration in the bulk feed. Consequently, at steady state, the solute concentration in the boundary layer is higher than the solute concentration in the bulk feed. Solute diffusive flux in the boundary layer is away from the membrane, since diffusion occurs down a concentration gradient. Positive solute permeate flux can, therefore, only occur if solute convective flux towards the membrane in the boundary layer is greater than solute diffusive flux away from the membrane. When Equation 24 is used to assess the Peclet number, the Peclet number should be greater than one for this separation.
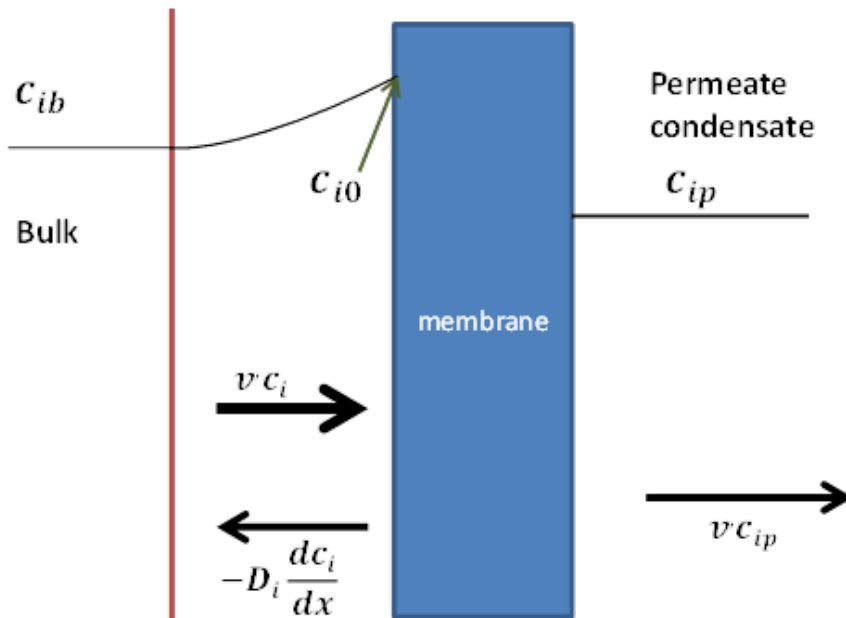

Figure 10.—Membrane desalination. Solute concentration profile. Relative contributions of convective and diffusive solute flux in the boundary layer to permeate flux.

Flux in the boundary layer is the sum of the convective and diffusive flux. In pervaporation desalination, the diffusive flux is away from the membrane as shown in Figure 10.

NaCl concentration in the permeate vapor is close to zero. The concentration profile ($c_{ib} > c_{i0} > c_{i0p}$) must exist to use the RIS model (Equation 42). Positive solute flux is generated by the convective component in pervaporation desalination. This is true because in pervaporation desalination, $c_{i0} > c_{ib}$, solute diffusion is away from the membrane.

Employing a Sherwood correlation is the most widely used way to determine the SBLMTC in membrane desalination. Sherwood correlations are used to obtain the SBLMTC in VOC separation from water. The result of a Sherwood correlation can be verified in that separation using the RIS model methodology. It is therefore desirable to develop an alternate methodology to obtain the SBLMTC for membrane desalination.

The governing equation for this alternative methodology, as described by Baker (2012), is obtained from the TFBLT, Equation 30. The numerator and denominator on the LHS of Equation 30 are divided by c_{ip}. Then the logarithm of both sides of the resulting equation is taken to obtain Equation 45 for membrane desalination (note that to derive a similar equation for VOC separations, the first and second terms in the numerator and denominator have to be switched to avoid taking the logarithm of a negative number):

Equation 45. $\ln\left(\frac{1}{E}-1\right) = \ln\left(\frac{1}{E_0}-1\right) - \left(\frac{v'\delta}{D_i}\right)$

E and E_0 in Equation 45 are defined by Equation 46 and Equation 47:

Equation 46. $E = \frac{c_{ip}}{c_{ib}}$

Equation 47. $E_0 = \frac{c_{ip}}{c_{i0}}$

To our knowledge, Equation 45 has not been previously described or used in the membrane desalination literature to date. Flux and rejection values at different temperatures, with other operating conditions (e.g. feed composition) remaining constant, are the data for this method (Baker et al. 2012).

Examination of Equation 45 shows that:

Equation 48. $\lim_{\delta \to 0} E = E_0$

Intrinsic enrichment is the enrichment found in the absence of a boundary layer and is a constant for a given membrane and feed concentration. A plot of Equation 45 results in a line. The 1st term on the RHS of Equation 45 is the

intercept, the 2nd term on the RHS is contains v', the independent variable, and, $\frac{\delta}{D_i}$, the reciprocal of the SBLMTC the slope. The LHS of Equation 45 is the dependent variable.

The second term on the LHS of Equation 45 is the product of the volumetric water flux, v', and the reciprocal of the SBLMTC, D_i/δ. This product is the Peclet number if Equation 25 is used. As discussed, semi-quantitative analysis of membrane desalination revealed that the Peclet number is greater than one for that separation.

Equation 45, a variant of the TFBLT equations, predicts that c_{ip} varies directly with v'. That is that rejection is inversely related to water flux in membrane desalination.

Equation 45 is not applicable when $c_{ip} = 0$ or $\delta = 0$. Equation 45 is not valid if the solute permeate concentration is zero because that would result in a zero in the denominator the fraction on the LHS of equation 45. Equation 45 is not valid in the absence of a boundary layer ($\delta = 0$).

The TFBLT Equation 45 can be applied to separations such as pervaporation desalination where the solute is enriched at the feed side membrane service and to separations such as the VOC separation from water where the solute is depleted at the feed side membrane surface. For example, Equation 45 was used to evaluate concentration polarization in VOC separation (Baker et al. 1997). Equation 45 was used here to evaluate concentration polarization by analyzing data from several papers on pervaporation desalination (Table 7).

2.7. Temperature Polarization in Pervaporation

A discussion of temperature polarization that normally occurs in pervaporation, as well as the reversal of temperature polarization seen in photothermal nanophotonic pervaporation is necessary to the understanding of the novel theory of how concentration polarization mitigation occurs.

According to Favre (2003), there are only a few studies on temperature polarization in pervaporation.

In Karlsson and Trägårdh (1996), temperature polarization was evaluated by using the Arrhenius expression for flux as shown in Equation 49:

Equation 49. $J_w = J_0 \exp\left(\frac{-E_a}{RT}\right)$

Where:
J_w is water flux [kg m^{-2} s^{-1}]
E_a is the activation energy of permeation [J mol^{-1}]

R is the gas constant [J mol^{-1} K^{-1}]

T is the "wall" (feed/membrane interface) temperature [K].

Karlsson and Trägårdh (1996) used a feed of pure water and set up their experiment so that the feed inlet and outlet temperatures were 75℃. Karlsson and Trägårdh found that the observed flux varied inversely with feed flow velocity. Then Equation 49 was used by Karlsson and Trägårdh to determine the "wall" temperature, i.e. the temperature at the feed side membrane surface. A temperature drop of 1.1 K was found for the lowest feed flow velocity.

Kuhn et al. (2009) modeled pure water pervaporation through a Linde Type A zeolite membrane using Maxwell-Stefan type equations. The reader is referred to the original study to view how the model was constructed. The result of the modeling was that, using a water feed temperature of 348 K and a flux of 0.15 $molm^{-2}s^{-1}$, they found a transmembrane temperature change of 1.3 K.

Favre (2003) uses a similar approach to Karlsson and Trägårdh to model temperature polarization for pure liquid feeds (water, ethanol, butanol, pentanol, ethyl propionate). In this case, the governing equation is Equation 50:

Equation 50. $J = J_0 \exp\left(\dfrac{-E_A}{R\left(T_b - \frac{\varphi}{h_0 + a\omega^\gamma}\right)}\right)$

Where:

J is flux of the pure liquid feed [kg m^{-2} s^{-1}]

E_A is activation energy of permeation [J mol^{-1}]

T_b is bulk feed temperature [K]

R is the gas constant [J mol^{-1} K^{-1}]

h_0 is the boundary layer heat transfer coefficient [W m^{-2} K^{-1}]

ω is the feed impeller rotational speed [s^{-1}]

φ is the transmembrane heat flux [W m^{-2}]

a and γ are fitting parameters [-].

h_0 is obtained by using a Nusselt correlation. φ is obtained by Equation 51:

Equation 51. $\varphi = J\Delta H_v$

Where:

ΔH_v is the enthalpy of vaporization for the permeating species [J kg^{-1}].

In Equation 50, the expression in parenthesis in the denominator on the RHS is the temperature at the feed/membrane interface, T_m [K] as shown in Equation 52:

Equation 52. $T_m = T_b - \dfrac{\varphi}{h_0 + a\omega^\gamma}$

Although Favre (2003) did not specify what values he obtained by his modeling for T_m he did show, for example, a significant effect on the calculated activation energy due to changes in the impeller rate.

As Favre points out, the mechanism for temperature polarization in pervaporation is similar to that of vacuum membrane distillation. Alsaadi et al. (2014), used pure water feeds. Alsaadi et al. (2014)'s modeling objective was to calculate the temperature polarization coefficient, TPC [-]:

Equation 53. $\text{TPC} = \frac{T_m - T_p}{T_b - T_p}$

Where:
T_p is the permeate side temperature [K]

The relationship in Equation 54 was used by Alsaadi et al. (2014) to obtain T_m:

Equation 54. $Q = h_0(T_b - T_m) = J\Delta H_v = \mathcal{P}_m(p_m - p_p)\Delta H_v$

Where:
$\mathcal{P}_m$ is the water permeance of the membrane [kg m^{-2} s^{-1} kPa^{-1}]
p_m is the water vapor pressure at the feed/membrane interface [kPa]
p_p is the permeate water vapor pressure [kPa]

As in Favre (2003), h_0 was obtained by Alsaadi et al. (2014) using a Nusselt correlation.

An iterative process was used by Alsaadi et al. (2014) to solve for T_m and the TPC. A linear relationship was found between TPC and T_b, with a TPC of about 0.9 at 20 ℃ and a TPC of about 0.7 at 95℃.

All of the studies discussed so far in this section found that the temperature at the feed/membrane interface was less than the bulk feed temperature. The difference between the bulk feed temperature and the temperature at the feed/membrane interface varied between the studies. In Karlsson and Trägårdh (1996) and Kuhn et al. 2009, the temperature difference was small (about 1 ℃) whereas in Favre (2003) and Alsaadi et al. (2014), the difference was larger. It is difficult generalize on the severity of temperature polarization in pervaporation based on these studies.

2.8. The Nanophotonic Photothermal Effect in MD and Pervaporation

Carbon black and noble metal nanoparticles can produce a photothermal effect. Gold nanoparticles exhibit plasmonic resonance. Jiang et al. (2013) document absorption peaks between 500 and 900 nm, depending on the size and

configuration of the gold nanoparticle. Jiang et al. (2013) and Dongare et al. (2017a) describe the light absorbance of carbon black as broadband (i.e., no peaks) between about 400 and 900 nm. Jiang et al. (2014) and Chen et al. (2010) also discuss the photothermal conversion efficiency, which is based on an energy balance conducted on noble nanoparticles while under illumination. However, it is not necessary to apply to membrane nanophotonics to quantify photothermal conversion efficiency. For example, Dongare et al. (2017a) used a Monte Carlo photon transport method, taking into consideration light scattering and absorption, to help arrive at the optimal carbon black (CB) concentration for photothermal DCMD.

Li et al. (2013) published a study in 2013 on incorporating silver nanoparticles in polydimethylsiloxane (PDMS) membranes to improve pervaporative ethanol (a VOC) separation from water using a 5 percent weight (wt%) ethanol feed. Silver nanoparticles were included into a thin PDMS membrane by an *in situ* method which was then layered onto a poly vinylidene fluoride (PVDF) support. The silver nanoparticles were found to have an absorption peak at about 400 nm, and a 400 nm light-emitting diode (LED) light at an intensity up to 920 Watts per square meter (Wm^{-2}) was used for their experiments. Details of the pervaporation setup did not include the pervaporation cell dimensions or feed flow rate—except to indicate that the membrane had a surface area of 120 square centimeters (cm^2). Results included improved flux and selectivity for the membranes, incorporating silver nanoparticles under irradiation compared to the same membranes with the light off. Li et al. (2013) did not include any measurement or modeling of the temperature profile within the membrane and boundary layer, although a diagram with a proposed mechanism showed the reversal of temperature polarization when the nanophotonic photothermal effect was in place.

Dongare et al. (2017a) used a membrane comprised of a thin (25 micron) carbon black coated porous polyvinyl alcohol (PVA) layer, coated onto a PVDF support. A 1% NaCl feed was used with a feed flow rate of 0.54 cubic centimeters per second ($cm\ s^{-1}$). This study of DCMD also had a permeate flow rate of 4.34 cm s^{-1}. The cell dimensions were 3.46x8.10x0.15 centimeters (cm). A 1 millimeter (mm)-thick quart plate was used to cover the feed channel. Tests were conducted in Houston, Texas, where the ambient solar intensity was 700 Wm^{-2}. Experiments were conducted with unfocused light and at 25x magnification. The fluxes were separated into the contributions from localized photothermal heating, the flux due to the experimental temperature difference between the bulk feed and distillate streams, and the flux due to residual heating of the system upon illumination. According to Figure S4 in Dongare et al. (2017a), the flux of the illuminated membrane was about 0.6 kg $m^{-2}\ h^{-1}$ after 10 minutes, about twice that of the unilluminated membrane under the same conditions. (These fluxes are low compared with those usually reported for conventional DCMD due to the small temperature difference between the feed and permeate, about 3-5 °C).

Dongare et al. (2017a) included an estimate of the energy efficiency of nanophotonic-enabled solar membrane distillation (NESMD). The measurement was based on the amount of distillate produced, and the enthalpy of vaporization, compared with the incident solar power. Dongare et al. (2017a) reported an efficiency of 21.45 % for the unfocused condition and 21% for the focused condition. A simulation showed that for the unfocused condition, the temperature at the feed/membrane interface was about 1 °C higher than the bulk feed. However, additional simulations, unpublished, reported at the recent Industrial Practitioners Advisory Board (IPAB) meeting by the Dongare et al. 2017b showed about a 75 °C local difference when 10x magnifying lenses were used. Significant findings included:

1) NESMD was more efficient at lower feed velocities (opposite to conventional DCMD)

2) The average distillate flux increased with the length and width of the module (opposite to conventional DCMD)

3) The solar energy efficiency of NESMD improved with increased ambient temperature

Politano et al. (2017) conducted a study of photothermal VMD for seawater desalination. They used silver nanoparticles (NPs) incorporated into a microporous poly vinylidene fluoride (PFDF) membrane. The maximum absorbance for silver is nanoparticles (NP) is at about 420 nm. For this study, an ultraviolet (UV) lamp with an emission wavelength of 365 nm and an intensity (at the distance from the VMD cell) of 23,000 watts per square meter (Wm^{-2}) was used. The feed was either pure water or 0.5 M NaCl. The feed volumetric flow was 5.5 cm^3 s^{-1}. The membrane surface area was 21.21 cm^2. The initial feed temperature was 303 K. For the purpose of calculating the temperature at the feed/membrane interface, T_m, two equations were used. Equation 55 is the energy balance:

Equation 55. $q_r + q_p = q_v + (q_{f,out} - q_{f,in})$

Where:
q_r is the heat flux due to irradiation from the UV lamp [W m^{-2}]
q_p is the plasmonic heat flux [W m^{-2}]
q_v is the heat flux required to vaporize water [W m^{-2}]
$(q_{f,out} - q_{f,in})$ is the heat flux through the liquid feed stream [W m^{-2}]

Equation 56 is similar to that used by Favre, except a plasmonic heating term is used:

Equation 56. $h_0(T_b - T_m) + q_p = J_w \Delta H_v$

The results include an increase in flux from 2.2 kg m^{-2} h^{-1} using an irradiated uncoated membrane to 25.7 kg m^{-2} h^{-1} using a 25% silver NP membrane. In the latter case, T_m rose to 327.3 K, about a 23 K increase above the baseline feed temperature, producing a TPC greater than 1. For unloaded PFVD membranes, the bulk feed temperature was raised about 2.5 K while for the 25% silver NP membranes the bulk feed temperature was raised about 4 K.

The boundary layer temperature polarization profiles for uncoated membranes (the baseline case) and for nanophotonic particle coated membranes having a photothermal effect are shown in Figure 11.
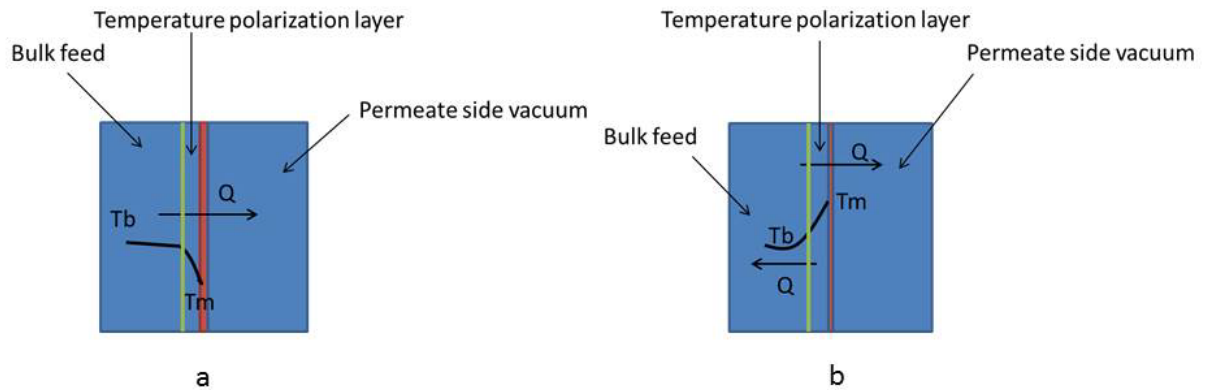
Figure 11.—The boundary layer temperature profile in (a) a non-illuminated coated or uncoated membrane, and (b) an illuminated coated membrane.

2.9. The Mitigation of Concentration Polarization in Photothermal Pervaporation Desalination

The mitigation of concentration polarization is a simple theory. It is novel in that it has not been previously described.

As shown in Politano et al. (2017), the bulk feed is heated by the nanophotonic photothermal effect in excess of the irradiative heat supplied directly to the bulk feed by the light source. In our lab, we are conducting a case study based on the pervaporation cell to investigate the nanophotonic photothermal effect. The pervaporation cell is shown in Figure 12.
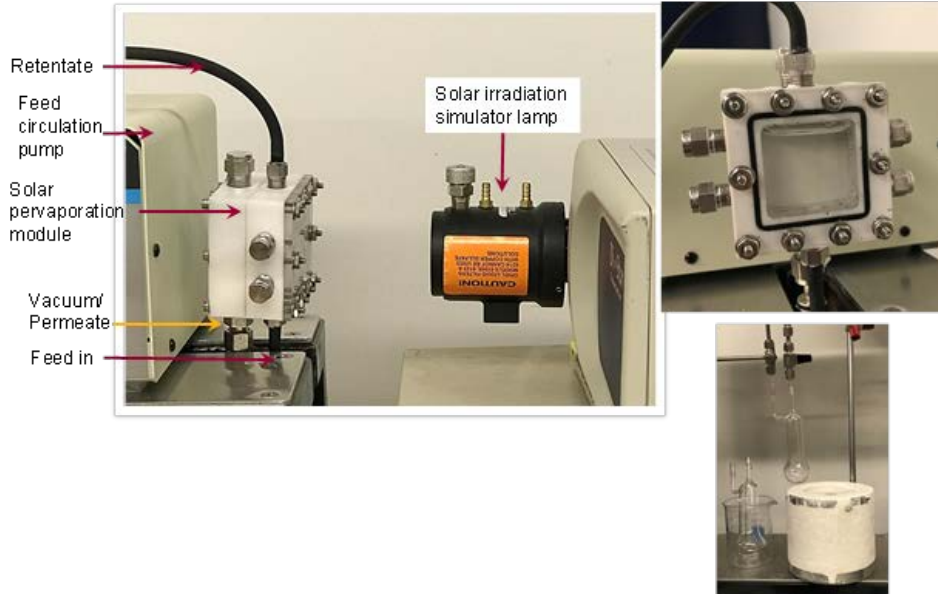
Figure 12.—Lab setup for solar pervaporation.

The solar cell is 4.5x4.5x2 cm, holding a volume of 40.5 cubic centimeters (cm^3).

The following are assumed conditions:
To start, assume pervaporation at 25 °C using dilute saline solution ($\rho \cong 1 \; g/cm^3$) as a feed for one hour. The feed is circulated by a pump, and the volume of fluid in the tubing is negligible. The membrane is nanophotonic enhanced, and a solar source is employed. The nanophotonic heating of the membrane results in enhanced flux, and the heat also creates a boundary layer at the feed/membrane interface with a temperature of 27 °C. The concentration polarization boundary layer thickness is 20 micrometers (μm). This assumption is the same as made by Baker (2012) in his chapter on concentration polarization (i.e., assume that the temperature polarization and concentration polarization layers have the same thickness.) This results in a boundary layer volume of 4.5x4.5x0.002 cm or 0.0405 cm^3. Assume that the temperature gradient that exists between the boundary layer and the bulk feed causes the bulk feed to rise in temperature by 1 °C due to convective heat transfer between the boundary layer and the bulk feed. C$_p$ of water is 4.1813 J g^{-1} K^{-1}. Then the enthalpy change of the bulk feed, ΔH [J], is shown in Equation 57:

Equation 57. $\Delta H = 4.1813 \; \frac{J}{gK} *1°K*40.5 \text{ g}$

 (This neglects the loss of feed volume, 2-3 g, due to flux)
$$\Delta H = 169 \, J$$
The heat flow to the bulk feed, Q [J s^{-1}], is:
$$Q = \frac{169 \, J}{3600 \, s}$$
$$Q = 0.047 \, \frac{J}{s}$$

The mass flow rate from the boundary layer, m [g s^{-1}] is shown in **Equation 58**:

Equation 58. $m = \frac{Q}{C_p \Delta T}$

$$m = \frac{0.047 \; J/_s}{4.1813 \; J/_{gK} \; 1°K}$$

$$m = 0.01125 \; \frac{g}{s}$$

The volumetric flow from the boundary layer, V [cm^3 s^{-1}] is:

$$V = 0.01125 \; \frac{cm^3}{s}$$

Therefore, the entire volume of the boundary layer is exchanged:

$$Boundary \; layer \; exchange \; rate = \frac{0.0405 \; cm^3}{0.01125 \; cm^3/_s}$$

$$Boundary \; layer \; exchange \; rate = 3.6 \; s$$

The entire boundary layer volume is exchanged by convection approximately every 3.6 seconds. This can be thought of as convectively stirring of the boundary layer.

2.10. Analytical Approach for Evaluating Concentration Polarization in Pervaporation Desalination

To study the severity of concentration polarization in pervaporation desalination, five published studies on pervaporation desalination were retrospectively analyzed (Malekpour et al. 2011, Drobek et al. 2012, Lin et al. 2012, An et al. 2014, and Naim et al. 2015). The published studies included four studies using inorganic membranes and one study using a polymer membrane. To use Equation 45, it was necessary to acquire flux and rejection data at various temperatures, with other operating conditions constant. The data acquired from the five published studies is presented in Table 7. Water flux in the five studies was reported in units of kg m^{-2} h^{-1}. This was converted to m s^{-1} by assuming a permeate density of 1 g cm^{-3}. The rejection data from the studies was used to obtain the solute permeate concentrations by using the solute bulk feed concentrations provided in the studies. Then enrichment (E) was computed using Equation 46. The enrichment values obtained were placed in the LHS of Equation 45, and the flux values [m s^{-1}] were placed in the RHS of Equation 45. In the linear plots obtained, the intercept gives the intrinsic enrichment, E_0 [-], (Equation 47) and the slope gives the Peclet number [-] (Equation 25). The Peclet number [-] is then used to compute the concentration polarization modulus C' [-] (Equation 26).

Table 7.—Input Values for Equation 45 from Desalination Studies

Citation	Feed	Membrane material	T ℃	v' [m s^{-1}]*10^7	ln(E^{-1}-1) [-]
Naim et al. 2015	140 g/L NaCl	cellulose acetate	50	5.28	5.76
			60	6.94	4.30
			70	10.40	2.44
			80	8.33	5.34
An et al. 2014	1.4 g/L NaCl	Clinoptilolite phophate	23	19.40	3.32
			50	27.80	3.28
			75	33.30	2.84
			95	41.70	1.89
Lin et al. 2012	35 g/L NaCl	Cobalt oxide silica	20	0.88	6.90
			50	1.81	5.80
			75	3.33	4.70
Drobek et al. 2012	75 g/L NaCl	Silicalite-1	20	4.86	5.29
			50	5.56	4.60
			75	8.33	3.89
Drobek et al. 2012	150 g/L NaCl	Silicalite-1	20	4.17	4.60
			50	4.86	4.18
			75	6.25	3.66
Malekpour et al. 2011	0.001 M/L CsNO$_3$	NaA	25	0.64	4.98
			40	0.66	4.95
			50	0.76	4.93
			65	0.90	4.95
Malekpour et al. 2011	0.001 M/L NaI	NaA	25	0.32	6.10
			40	0.33	6.00
			50	0.33	6.00
			65	0.36	5.80
Malekpour et al. 2011	0.001 M/L Sr(NO$_3$)$_2$	NaA	25	0.60	5.08
			40	0.63	5.05
			50	0.65	5.01
			65	0.70	4.95

2.11. Methodology for Applying the Debye-Huckel Theory to Obtain Ion Activity Coefficients and Activities

This section presents a brief discussion on how to obtain ion activities. As is well known, the solubility product of sparingly soluble salts is used to predict, from a thermodynamic viewpoint, whether precipitation will occur. Often, ion concentrations are used to compute the solubility product, which then, along with the associated constant, is used to predict whether precipitation will occur. As will be shown, this is a simplification which essentially is only valid at low concentrations. A more vigorous approach involves using ion activities to compute the solubility product. Debye-Huckel theory (Stumm and Morgan 1996) is used to obtain ion activity coefficients which, together with the ion mole fractions, are used to obtain activities. Equation 61 is used to obtain the ion activity coefficient, γ [-]:

Equation 59. $log_{10}\gamma = \frac{-0.51z^2\sqrt{I}}{1+3.288a\sqrt{I}} + bI$

Where:
γ is the activity coefficient [-]
I is the ionic strength [mol L^{-1}]
z is the ion valence [-]
a [nm] and b [L mol^{-1}] are ion specific parameters

Equation 62 is used to compute the ionic strength [mol L^{-1}]:

Equation 60. $I = \frac{1}{2}\sum C\,z^2$

Where:
C is the individual ion concentration [mol L^{-1}].

Table 8 provides the values for the Debye-Huckel constants for use in Equation 61. Activities are calculated according to Equation 63:

Equation 61. $a = \gamma x_i$

Where:
a is activity
x_i is the ion mole fraction [-]

**Table 8.—Values for Debye-Huckel Constants**

Ion component	a [nm]	b [L mol⁻¹]
Na	0.4	0.075
Ca	0.6	0.165
Mg	0.65	0.2
K, Cl	0.3	0.015
SO4	0.4	-0.04
HCO3	0.54	0

The results of the activity coefficient calculations for the ions in Table 8 are presented below as plots of activity coefficient, γ [-], compared to ionic strength, I, [mol L⁻¹].

# 2.12. Methodology for Synthesizing and Testing Nanophotonic Pervaporation Membranes

We obtained asymmetric membranes with a PVA separation layer from DeltaMem. Figure 13 presents a cross-sectional schematic and electron micrograph showing the details of the membrane structure. These membranes are marketed as hydrophilic membranes for dehydrating alcohols.
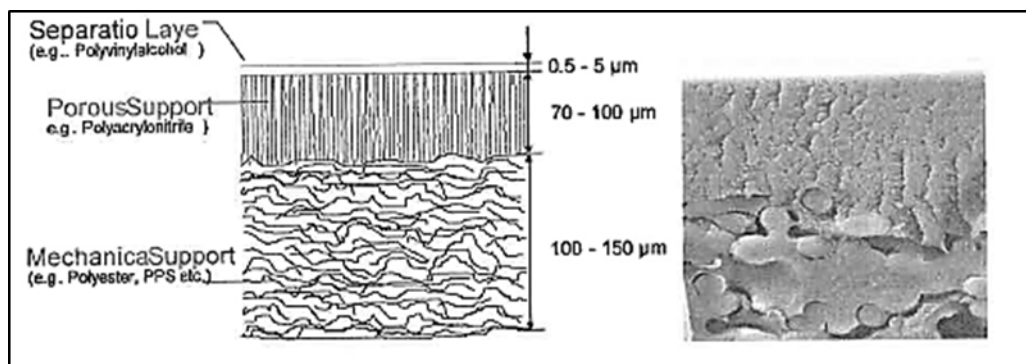
Figure 13.—Diagram of asymmetric PVA membranes obtained from DeltMem.

The nanophotonic material we used to make nanophotonic pervaporation membranes was 350 nm carbon black, (Emperor). The synthesis technique is simple. A paste made of carbon black (1.4 g), water (0.2 g), and tetrahydrofuran (THF) (1.3 g) is painted onto the 4155-40 or 4155-80 membranes. The painted membrane is allowed to dry overnight under a vacuum hood and then is suitable for pervaporation testing. Figure 14. compares scanning electron microscope (SEM) for the coated and uncoated membranes.
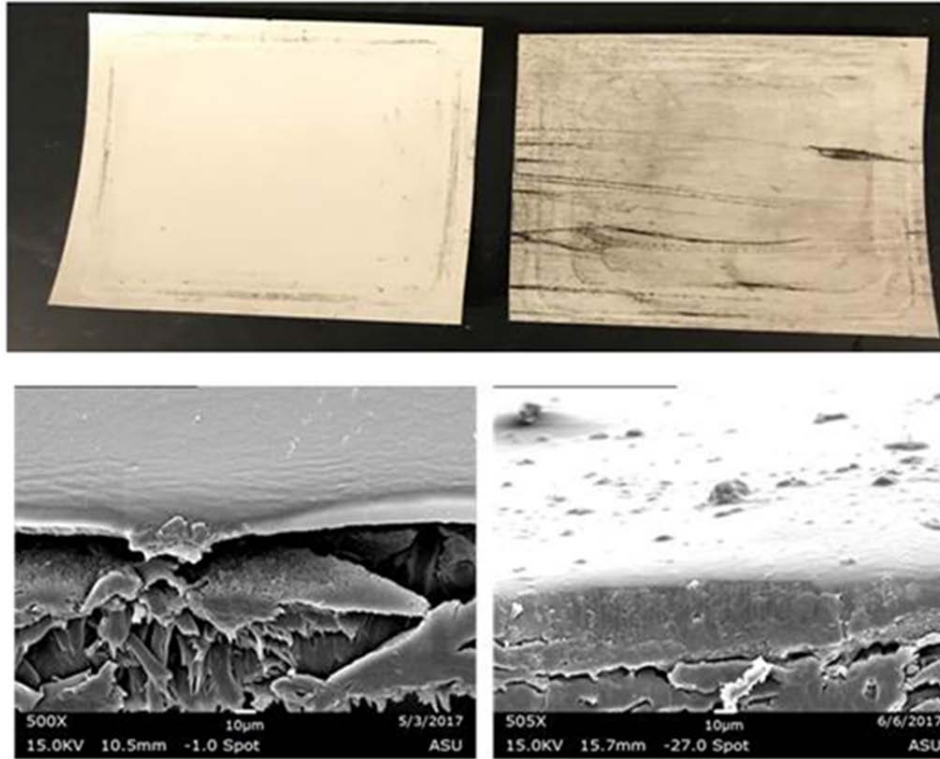
Figure 14.—Uncoated (left) and CB coated (right) DeltaMem membranes as shown with SEM.

In the pervaporation experiments to test the efficacy of the nanophotonic coating, we used a solar simulator lamp (Di Star 300 W Xenon lamp). The solar light source supplied light at an intensity of approximately 3,000 Wm^{-2} (3 suns), as determined by a Thor labs PM100D - Compact Power and Energy Meter Console.

The pervaporation cell used for the experiments is shown in Figure 12 and is described above.

Four pervaporation tests were done with a 32 g L^{-1} feed at room temperature to show the flux improvement imparted by the nanophotonic (CB) layer:

1) Pervaporation with uncoated membrane, no solar light
2) Pervaporation with uncoated membrane with solar light
3) Pervaporation with coated membrane, no solar light
4) Pervaporation with coated membrane with solar light

3. Results

3.1. Pervaporation Desalination Literature Analysis Results and Discussion

The results of the application of Equation 45 are shown in, Figure 15, Figure 16, Figure 17, Figure 18, Figure 19, Figure 20, Figure 21, and Figure 22, as well as Table 9 and Table 10. The figures all show a negative slope, which is equal to the negative reciprocal of the solute boundary layer mass transfer coefficient D_i/δ. The intercept of the plot in each figure is equal to $\ln((1/E_0) - 1)$ giving the intrinsic enrichment E_0. The linear fit of the data shown in the plots is in general strong with the lowest R-square equal to 0.8412.
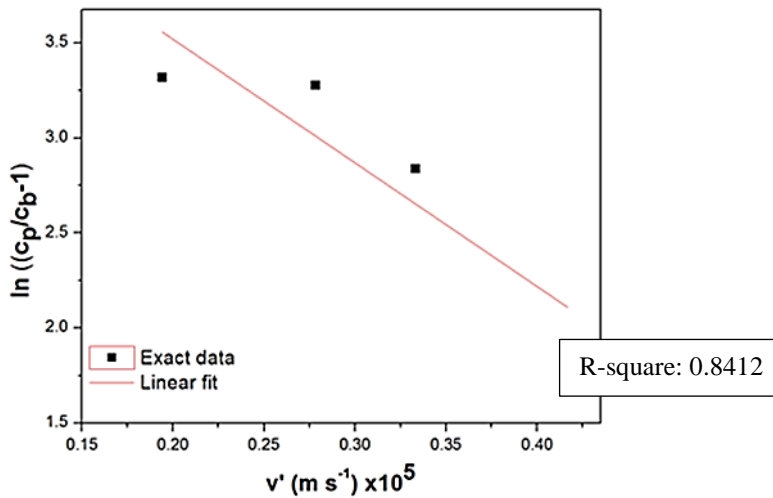
Figure 15.—An et al. (2014) TFBLT data representation (points) and linear best fit.
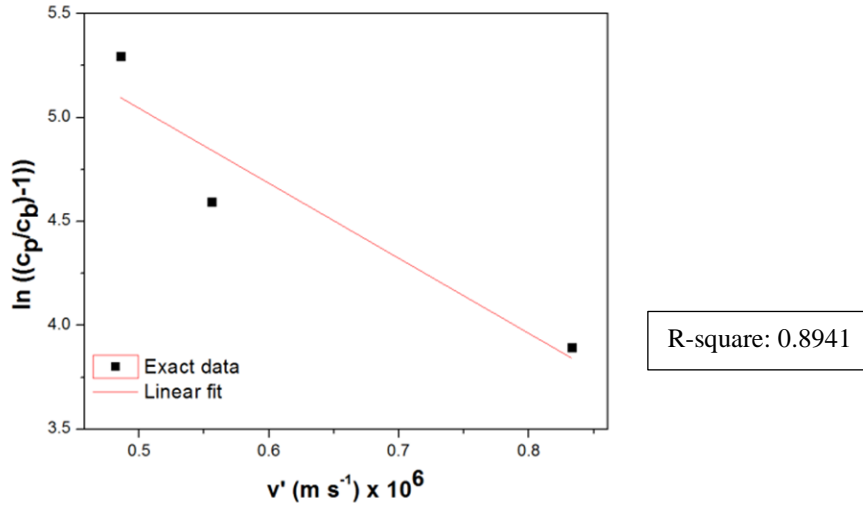
Figure 16.—Drobek et al. (2012) 7.5 wt.% NaCl feed. TFBLT data representation (points) and linear best fit.
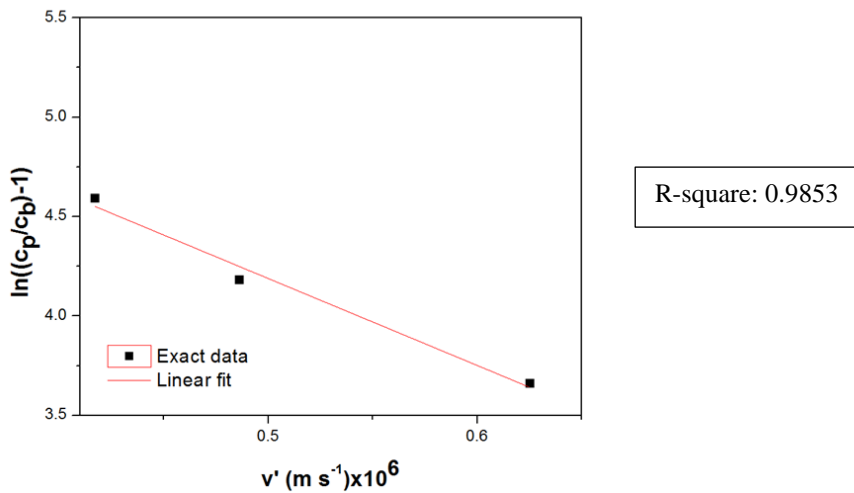

Figure 17.—Drobek et al. (2012) 15 wt.% NaCl feed. TFBLT data representation (points) and linear best fit.
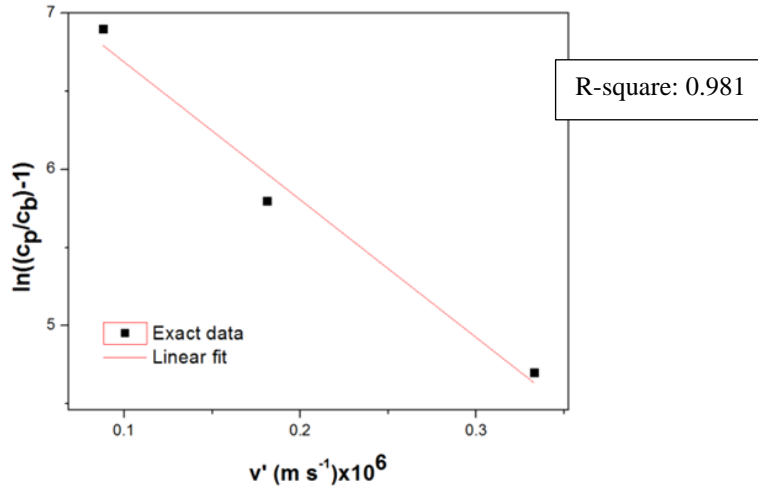
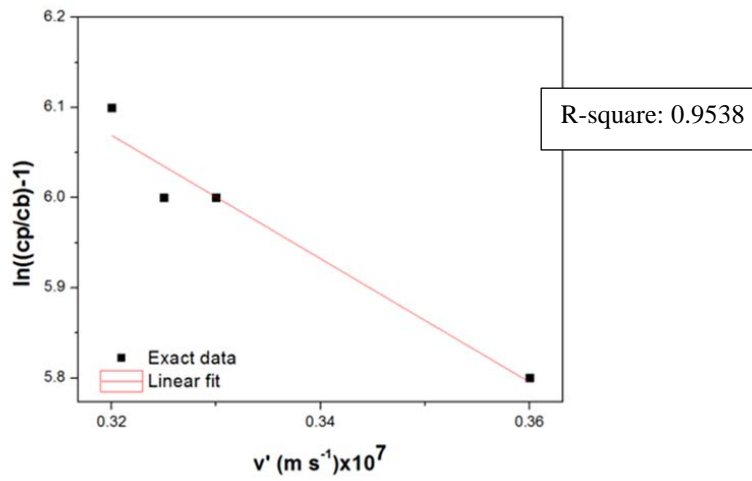**Figure 18.—Lin et al. (2012) TFBLT data representation (points) and linear best fit.**

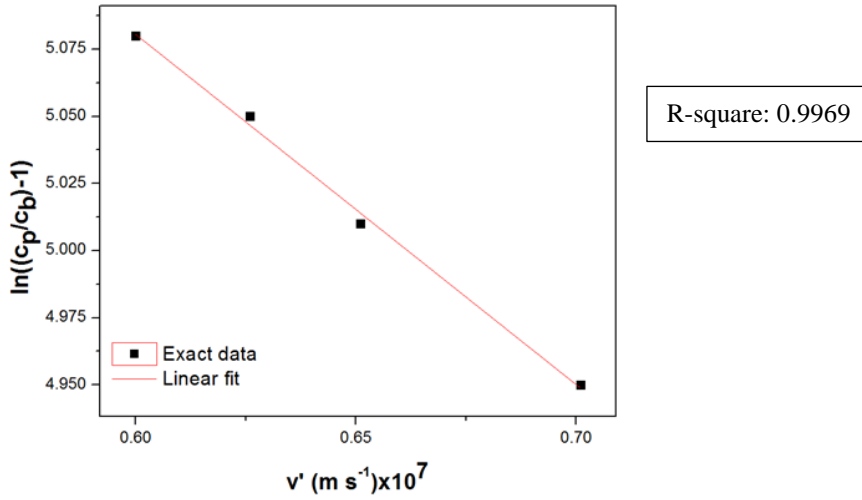**Figure 19.—Malekpour et al. (2011) NaI feed. TFBLT data representation (points) and linear best fit.**

Figure 20.—Malekpour et al. (2011) Sr(NO$_3$)$_2$ feed. TFBLT data representation (points) and linear best fit.

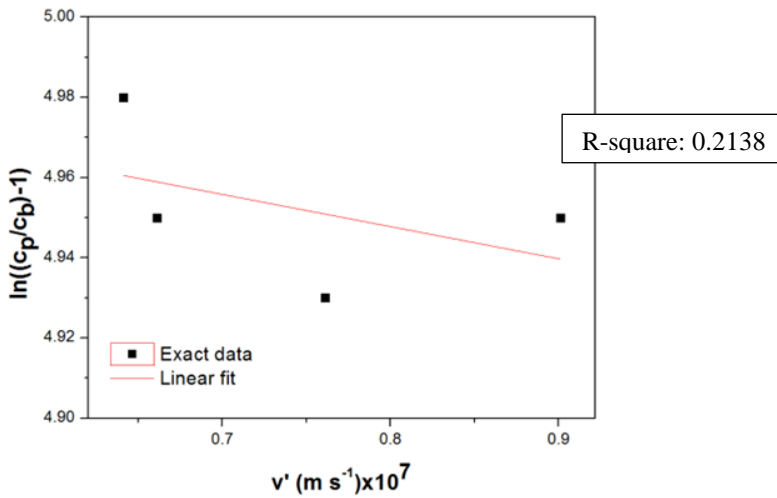**Figure 21.—Malekpour et al. (2011) Cs(NO$_3$) feed. TFBLT data representation (points) and linear best fit.**
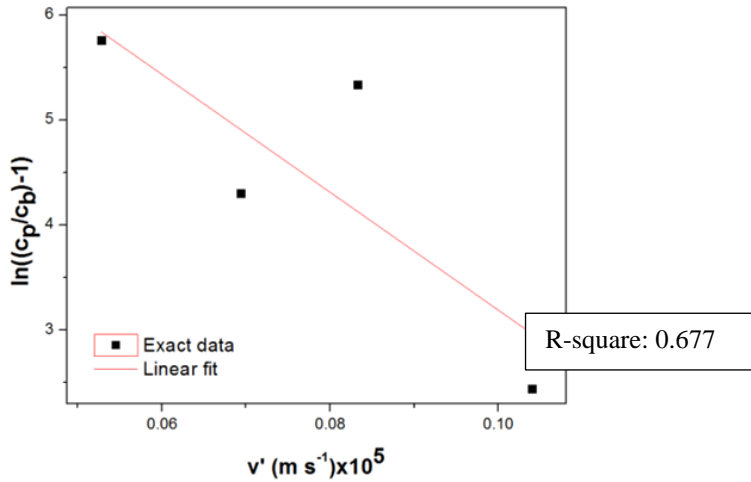
Figure 22.—Naim et al. (2015) TFBLT data representation (points) and linear best fit.

Table 9.—Reciprocal Boundary Layer Mass Transfer Coefficient, Peclet Number, Concentration Polarization Modulus, Intrinsic Enrichment; Calculated from Data From Previously Published Studies on Pervaporation Desalination

Citation	δ/D_i [s m^{-1}]*10^{-6}	$\frac{v'\delta}{D_i}$ [-]	C' [-]	E$_0$ [-]*10^3
Niam et al. (2015)	5.61	2.96-4.68	19.4-107	0.30
An et al. (2014)	0.65	1.26-2.71	3.53-15.1	0.80
Lin et al. (2012)	8.81	0.78-2.93	2.17-18.8	0.50
Drobek et al. (2012)[*]	3.61	1.76-3.19	5.79-24.3	1.00
Drobek et al. (2012)[**]	4.33	1.82-2.73	6.19-15.4	2.00
Malekpour et al. (2011)[#]	0.80	0.05-0.07	1.05-1.07	7.00
Malekpour et al. (2011)[##]	68.39	2.19-2.46	8.92-11.7	0.30
Malekpour et al. (2011)[###]	13.94	0.78-0.91	2.19-2.490	3.00

*7.5 wt% NaCl feed **15 wt% NaCl feed
#0.001 M/L CsNO$_3$ feed ##0.001 mol/ L NaI feed ###0.001 mol/ L Sr(NO$_3$)$_2$ feed

Table 10.—Effect of Concentration Polarization on Observed Flux In Pervaporation Desalination

Citation	Feed g L^{-1}	Bulk feed water mole fraction	Mole fraction water at feed/membrane interface	Observed Flux kg m^{-2} h^{-1}	Flux in absence of concentration Polarization kg m^{-2} h^{-1}
Niam et al. (2015)	40	0.988	0.42	5.97	13.75
Lin et al. (2012)	35	0.989	0.81	1.2	1.5
An et al. (2014)	1.4	0.99	0.99	15	15
Drobek et al. (2012)	3	0.99	0.99	11.5	11.5

The following observations can be made based on the data:

1. The pervaporation desalination results, derived from the thin film boundary layer theory (Baker's method) in general conform to the semi-quantitative prediction of $(\frac{v'\delta}{D_i})$ greater than one. The reason that some of the values of $\frac{v'\delta}{D_i}$ are less than one is not known. One explanation is that the assumption that v' represents the convective solute flux may not be correct for desalination.

2. Analysis of the data from Drobek et al. (2012) show that for the same flux, the polarization effect is worse at higher feed concentration.

Lin et al. (2012) studied a 35 g/L NaCl feed, which is representative of a seawater feed. The bulk feed water mole fraction is 0.989. At 75 °C, the concentration polarization modulus was 18.8—which results in a water mole fraction at the feed/membrane interface of 0.811. Thus, the observed flux is about 80% of what would have been realized without concentration polarization. These results suggest that concentration polarization in pervaporation desalination may be a serious problem, especially at the high solute concentrations found in RO concentrates.

3.2. Results of Excel Modeling of Concentration Polarization in RO and Pervaporation Desalination

The results of the modeling of concentration polarization are summarized in Figure 23 with a water mass transfer coefficient (WMTC) [L m^{-2} h^{-1} bar^{-1}]. The values for the WMTC presented in Figure 23 are representative of those presented in the last column of Table 2. The values of the WMTC chosen for Figure 23 are in the low to moderate range of the values found in the last column of Table 2. To convert the water permeance values presented in Table 2 [mol m^2 s^{-1} Pa^{-1}] to [L m$^-$

^{2} h^{-1} bar^{-1}] the reader can simply multiply the water permeance values in Table 2 (exclusive of the exponent multiplier) by 36/55.5.

|	Pervaporation								Reverse Osmosis
	Water Mass Transfer Coefficient, k_w = 13.9 L m^{-2} h^{-1}			Water Mass Transfer Coefficient, k_w = 160 L m^{-2} h^{-1}					
	Feed Temperature °C			Feed Temperature °C					Feed Temp °C
	25	50	75	25	50	75			20
Reynolds exponent	C'	C'	C'	C'	C'	C'	Reynolds exponent		C'
0.83*	1.00-1.00	1.01-1.01	1.02-1.02	1.02-1.02	1.06-1.09	1.22-1.84	0.83*		1.11-1.14
0.3**	1.02-1.02	1.09-1.09	1.32-1.33	1.30-1.31	1.30-1.31	23.5-77.4	0.3**		2.6-3.4
0.35	1.02-1.02	1.07-1.07	1.24-1.25	1.22-1.23	1.22-1.23	11.5-55.8	0.35		2.3-2.8
0.4	1.01-1.01	1.05-1.05	1.18-1.18	1.17-1.17	1.83-1.20	6.60-35.2	0.4		2.0-2.4
* from MWH									
**representative values based on pervap desal literature									

Figure 23.—C' [-] values obtained from excel model for RO and Pervap as function of Re number.

Figure 23 shows that concentration polarization is minimal in RO but can be severe in pervaporation desalination, particularly at larger fluxes or WMTCs. Larger WMTCs translate into larger fluxes which, in turn, result in larger Peclet numbers and concentration polarization moduli. Additional data is available on request contains numerous spreadsheets. This data shows that the propensity for scaling exists in both RO and pervaporation desalination when feeds containing calcium are used (e.g., calcium carbonate and calcium sulfate scaling). Clearly, the propensity for scaling is worse in pervaporation desalination with an RO concentrate feed and where significant concentration polarization exists.
It should be noted that the model is a thermodynamic model (i.e., an equilibrium model). It predicts when scaling will *eventually* occur but whether scaling will actually occur at all also depends on kinetics or residence time.

3.3. Results of Debye-Huckel Calculations

Figure 24 show plots of ionic strength vs. activity coefficient for the ions shown (calcium, bicarbonate, chlorine, potassium, sulfate, and magnesium). The ion specific parameters, **a** and **b** found in Table 8 are used in Equation 61 to create the individual ion plots. It can be seen from the plots that, in most cases, the activity coefficients (and activities) fall sharply with increasing ionic strength.
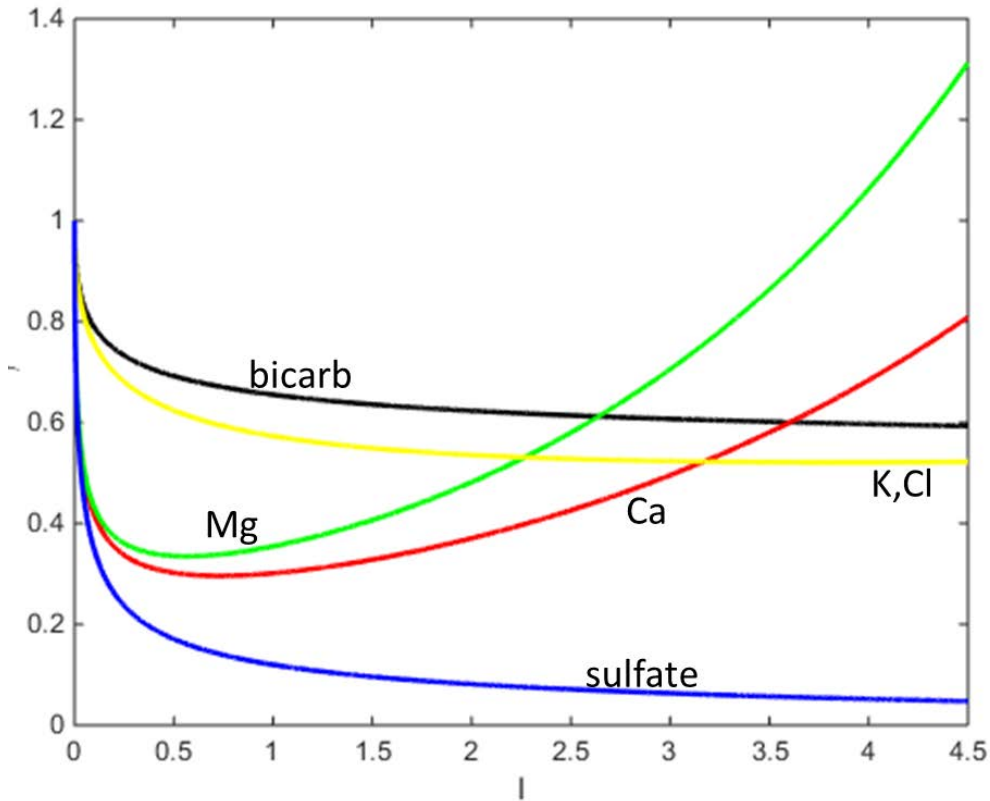
Figure 24.—Ion activity as a function of ionic strength.

The difference between activities and concentrations is illustrated in Table 11. Table 11 shows the results of analysis of a BGNDRF pervaporation desalination retentate obtained from our Excel modeling. The BGNDRF retentate (TDS of 29,362 mg/L) was obtained by running the BGNDRF feed (Table 5) through the pervaporation portion of our Excel model. The difference between activities and concentrations is significant (e.g., the sulfate activity is about 14% of the concentration).

Table 11.—BGNDRF Pervaporation Retentate, TDS=29362 mg/L, I=0.768

Component	Ion concentration mol L^{-1}		Activity
Na	0.171	0.71	0.12
Ca	0.08	0.3	0.026
Mg	0.066	0.34	0.022
Cl	0.16	0.59	0.095
SO$_4$	0.146	0.14	0.02
HCO$_3$	0.029	0.67	0.019

3.4. Results of Experiments on Nanophotonic Enhanced Pervaporation Desalination

The results of pervaporation experiments demonstrating the efficacy of the nanophotonic (carbon black) layer applied to the commercial DeltaMem membranes are shown in Figure 25, Figure 26, and Figure 27.
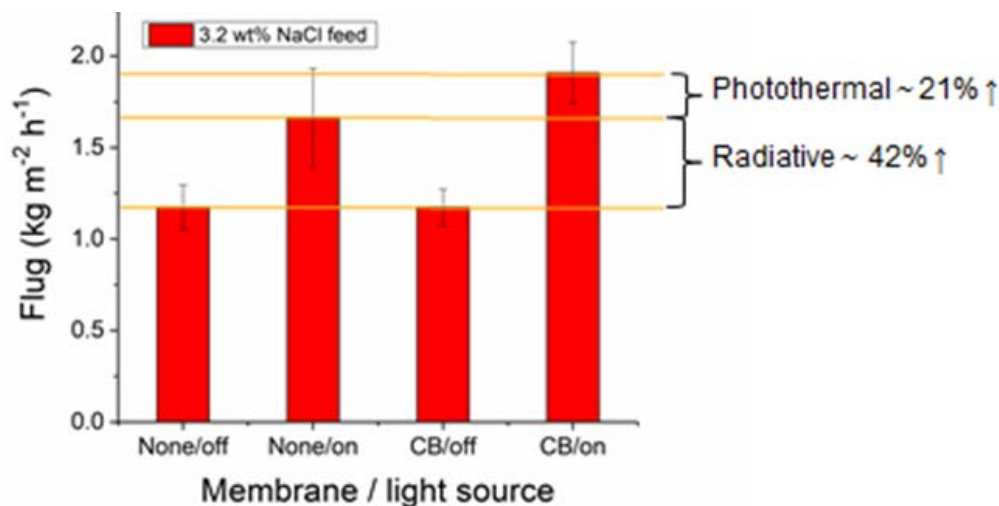

Figure 25.—Pervaporation of 32 g L^{-1} NaCl feed waters.

The average result of three trials using a 32 g L^{-1} NaCl feed at room temperature is represented in Figure 25. The flux of the uncoated and carbon black coated membrane without exposure to the light source was about the same. The flux of the uncoated membrane with exposure to the light source was about 42% higher than the flux of the uncoated or coated membrane without exposure to the light source due to radiative heating of the feed by the light source. The flux of the carbon black coated membrane with exposure to the light source was about 21% higher than the flux of the uncoated membrane with exposure to the light source due to the photothermal effect and about 62% higher than the flux of the uncoated or coated membrane without exposure to the light source due to both radiative heating and the photothermal effect. All measured rejections for the membranes reported in Figure 25 are greater than 99.9%.
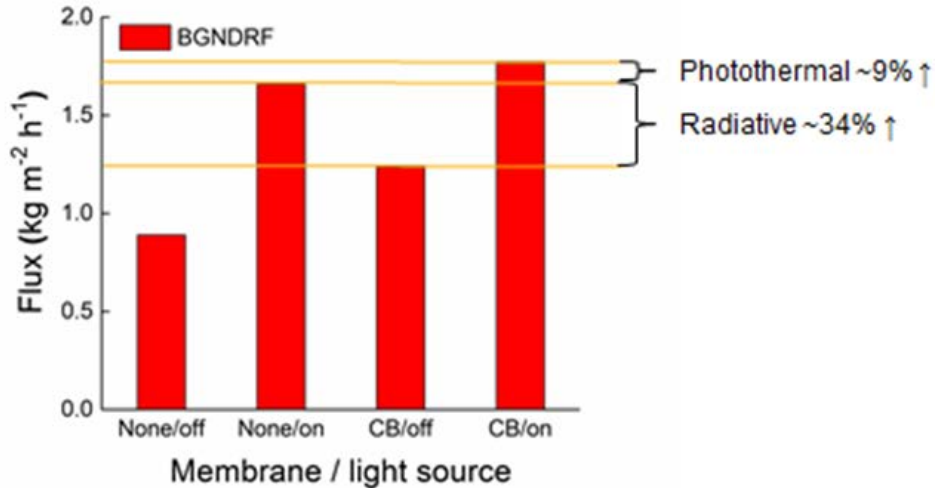
Figure 26.—Pervaporation of simulated BGNDRF water (TDS 4,035 mg L^{-1}).

The result of a single trial using a simulated BGNDRF feed with a TDS of 4,035 mg L^{-1} (see Table 5) is shown in Figure 26. There is a difference between the flux of the uncoated and carbon black coated membrane without exposure to the light source. This difference is unexplained but may be mitigated by further trials. The flux of the uncoated membrane with exposure to the light source was about 34% higher than the flux of the carbon black coated membrane without exposure to the light source to radiative heating. The flux of the carbon black coated membrane with exposure to the light source was about 9% higher than the flux of the uncoated membrane with exposure to the light source due to the nanophotonic effect and about 43% higher than the carbon black coated membrane without exposure to the light source, due to both radiative heating and the photothermal effect.
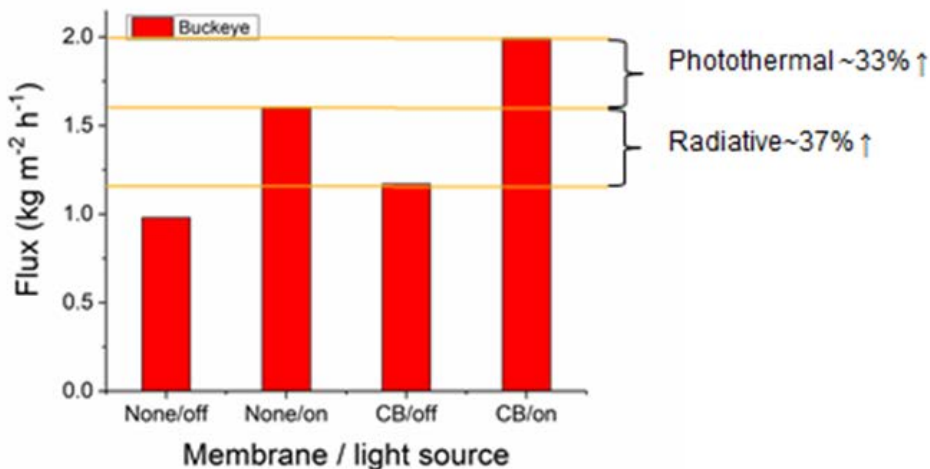

Figure 27.—Pervaporation of simulated Buckeye water (TDS 1583 mg L^{-1}).

The result of a single trial using simulated Buckeye well water with a TDS of 1,583 mg L^{-1} (see Table 5) is shown in Figure 27. The flux of the carbon black coated membrane without light exposure was about 10% higher than the flux of the uncoated membrane without light exposure. The flux of the uncoated membrane with light exposure was about 37% higher than the flux of the carbon black coated membrane without light exposure due to the radiative effect. The flux of the CB coated membrane with light exposure was about 37% higher than the flux of the uncoated membrane with light exposure due to the photothermal effect and about 70% higher than the carbon black coated membrane without light exposure due to both the radiative and photothermal effects.

The overall results show a high radiative heating effect. This is most likely due to the feed configuration. We did not use a feed reservoir. The solar cell (see Figure 12) holds about 40.5 cc and the connecting tubing holds about 10 cm^3. This means than when the light source is on the feed is exposed to the light 40.5/50.5 percent of the time.

A significant photothermal effect was demonstrated in all cases. That is, a significant increase in flux beyond that obtained by irradiation of the feed was obtained by adding a nanophotonic (carbon black) layer to the membranes.

4. Conclusions

Our literature analysis of pervaporation desalination shows that concentration polarization can be significant in some cases. We illustrated two examples (Table 10) where water flux was significantly impaired by concentration polarization. It was not possible to analyze the propensity for scaling in these studies because sparingly soluble salts were not included in the feeds. When the water permeance values (or WMTC values) and the intrinsic enrichment data were included in the model, we found that significant concentration polarization occurs at moderate values of the WMTC. Clearly, concentration polarization will worsen with even larger values of the WMTC. When better performing membranes are used the effect of concentration polarization will be even more significant than that illustrated here. There are two effects of concentration polarization:

1) Water flux impairment

2) Increased propensity for scaling

We showed that the effects of concentration polarization are mitigated—but not eliminated—when activities are used instead of concentrations. It can be expected that concentration polarization will be a significant problem when high concentration feeds such as RO concentrates are used in pervaporation desalination.

We developed first generation nanophotonic pervaporation membranes which have a significant photothermal enhancement of flux. The commercial membranes from DeltaMem that we used in this study were not designed for desalination. The highest flux we could achieve by conventional pervaporation using the DeltaMem membranes was about 1 kg m^{-2} h^{-1}. This is low in comparison with the values reported in the pervaporation desalination literature. MD is a competing technology. It is not possible to say, with a high degree of certainty, that the flux obtained by conventional MD is higher than that which can be achieved by conventional pervaporation desalination. We discussed the disadvantages of MD in terms of wetting, biofouling, and conductive heat loss (DCMD). The flux enhancement achieved by nanophotonic pervaporation desalination may be better than that which can be achieved by DCMD because there is no conductive heat loss through the membrane in pervaporation. In theory, water flux is enhanced by the photothermal effect because the heat emitted by the nanophotonic particles increases the feed side water saturation pressure and supplies the enthalpy of vaporization of water through the membrane. As stated, increased water flux will result in more concentration polarization.

However, we developed a theory on mitigating concentration polarization in pervaporation caused by photothermal heating of the membrane. Increased water flux and lower propensity for scaling will be obtained by concentration polarization mitigation.

5. Recommended Next Steps

We recommend that, in addition to treating water from concentrated inland brackish water RO brine solutions, future applications of nanophotonic enhanced pervaporation membranes be considered for other waters with solute-concentrations that exceed the limits of RO (e.g., produced wastewaters), in decentralized environments, and for the separations that are the main commercial use of pervaporation membranes. Specific areas of future research to further improve nanophotonic enhanced pervaporation desalination are:

1) Development of new dense pervaporation membranes that are actually optimized for desalination with higher baseline performance

2) Module-level innovations designed to allow nanophotonic membranes to have access to direct-solar light

3) Further studies into the scaling propensity and concentration polarization of the combined RO/pervaporation process.

6. References

Alkhudhiri A., N. Darwish, and N. Hilal. 2012. Membrane Distillation: A Comprehensive Review. Desalination. Volume 287, 15 February 2012, Pages 2-18. doi:10.1016/j.desal.2011.08.027.

Alsaadi A.S., L. Francis, G.L. Amy, and N. Ghaffour. 2014. Experimental and Theoretical Analyses of Temperature Polarization Effect in Vacuum Membrane Distillation. Journal of Membrane Science. Volume 471, 1 December 2014, Pages 138-48. doi:10.1016/j.memsci.2014.08.005.

An W., X. Zhou, X. Liu, P.W. Chai, T. Kuznicki, and S.M. Kuznicki. 2014. Natural zeolite Clinoptilolite-Phosphate Composite Membranes for Water Desalination by Pervaporation. Journal of Membrane Science. Volume 470, 15 November 2014, Pages 431-438. doi:10.1016/j.memsci.2014.07.054.

Ashoor B.B., H. Fath, W. Marquardt, and A. Mhamdi. 2012 Dynamic Modeling of Direct Contact Membrane Distillation Processes. In: 11th International Symposium on Process Systems Engineering. Computer Aided Chemical Engineering. Volume 31, 2012, Pages 170-174. doi:10.1016/B978-0-444-59507-2.50026-3.

Baker R.W., J.G. Wijmans, A.L. Athayde, R. Daniels, J.H. Ly, and M. Le. 1997. The effect of concentration polarization on the separation of volatile organic compounds from water by pervaporation. Journal of Membrane Science 137 159-172.

Baker R. 2012. Membrane Technology and Applications. Third Edition. (Wiley J, ed.).; 2012. 9780470743720. doi: 10.1002/9781118359686.

Bhattacharya S. and S. Hwang. 1997. Concentration Polarization, Separation Factor, and Peclet Number in Membrane Processes. Journal of Membrane Science. Volume 132, Issue 1, 20 August 1997, Pages 73-90. doi:10.1016/S0376-7388(97)00047-1.

Bolto B, M. Hoang, and Z. Xie. 2010. Pervaporation—A Further Low Energy Desalination Option? Water. 37. 77-79.

Bowen T.C., R.D. Noble, and J.L. Falconer. 2004. Fundamentals and Applications of Pervaporation through Zeolite Membranes. Journal of Membrane Science. Volume 245, Issues 1–2, 1 December 2004, Pages 1-33. doi:10.1016/j.memsci.2004.06.059.

Brian P.L.T. 1966 Mass Transport in Reverse Osmosis. In: Mertin, ed. Desalination by Reverse Osmosis. MIT Press.

Chaudhri S.G., B.H. Rajai, and P.S. Singh. 2015. Preparation of Ultra-Thin Poly(Vinyl Alcohol) Membranes Supported on Polysulfone Hollow Fiber and their Application for Production of Pure Water from Seawater. Desalination. Volume 367, 1 July 2015, Pages 272-284. doi:10.1016/j.desal.2015.04.016.

Chen H., L. Shao, and T. Ming. 2010. Understanding the Photothermal Conversion Efficiency of Gold Nanocrystals. Small. Volume 6, Issue 20. October 18, 2010. Pages 2272–2280. doi:10.1002/smll.201001109.

Côté P. and C. Lipski. 1988. Mass Transfer Limitations in Pervaporation forWater and Wastewater Treatment. In: Bakish R., ed. Proceedings of the Third InternationalConference on Pervaporation Processes in the Chemical Industry. Baksih Materials Corporation; pp. 449-462. Englewood, New Jersey.

Criscuoli A., M.C. Carnevale, and E. Drioli. 2008. Evaluation of Energy Requirements in Membrane Distillation. Chemical Engineering and Processing: Process Intensification Volume 47, Issue 7, July 2008, Pages 1098-1105. doi:10.1016/j.cep.2007.03.006.

Crittenden, J.C., R.R. Trussell, D.W. Hand, K.J. Howe, and G. Tchobanoglous. 2012. MWH's WaterTreatment : Principles and Design. Third Edition. (Wiley J, ed.) ISBN: 978-0-470-40539-0.

DeltaMem, 2017. Packaging information included with membranes, 2017

Desalitech. 2016. Desalitech Technology. Available at: http://desalitech.com/technology/.Accessed February 7, 2016.

Dongare P.D., A. Alabastri, S. Pedersen, et al. 2017a. Nanophotonics-Enabled Solar Membrane Distillation for Off-Grid Water Purification. Proceedings of the National Academy of Sciences. 2017 July, 114 (27) 6936-6941. doi:10.1073/pnas.1701835114.

Dongare P.D., A. Alabastri, S. Pedersen, et al. 2017b. Industrial Practitioners Advisory Board (IPAB) meeting, El Paso, Texas, October 2017.

Drobek M., C. Yacou, J. Motuzas, A. Julbe, L. Ding, and J.C. Diniz da Costa. 2012. Long Term Pervaporation Desalination of Tubular MFI Zeolite Membranes. Journal of Membrane Science. Volumes 415–416, 1 October 2012, Pages 816-823. doi:10.1016/j.memsci.2012.05.074.

Eykens L., K. De Sitter, C. Dotremont, L. Pinoy, and B. Van der Bruggen. 2016. How to Optimize the Membrane Properties for Membrane Distillation: A review. Industrial and Engineering Chemistry Research. 2016;55(35):9333-9343. doi:10.1021/acs.iecr.6b02226.

Fang Z., Y-R. Zhen, O. Neumann, et al. 2013. Evolution of Light-Induced Vapor Generation at a Liquid-Immersed Metallic Nanoparticle. Nano Letters. 2013;13(4):1736-1742. doi:10.1021/nl4003238.

Favre E. 2003. Temperature Polarization in Pervaporation. Desalination Volume 154 Issue 2 pages 129-138. doi:10.1016/S0011-9164(03)80013-9.

Feng X. and R.Y.M. Huang. 1994. Concentration Polarization in Pervaporation Separation Processes. Journal of Membrane Science. Volume 92, Issue 3, 25 July 1994, Pages 201-208. doi:10.1016/0376-7388(94)00056-5.

Feng X. and R.Y.M. Huang.1996. Estimation of activation energy for permeation in pervaporation processes. Journal of Membrane Science. Volume 118, Issue 1, 4 September 1996, Pages 127-131. doi:10.1016/0376-7388(96)00096-8.

Fouad E.A. and X. Feng 2008. Use of Pervaporation to Separate Butanol from Dilute Aqueous Solutions: Effects of Operating Conditions and Concentration Polarization. Journal of Membrane Science. Volume 323, Issue 2, 15 October 2008, Pages 428-435. doi:10.1016/j.memsci.2008.06.054.

Gekas V. and B. Hallström. 1987. Mass Transfer in the Membrane Concentration Polarization Layer Under Turbulent Cross Flow: I. Critical Literature Review and Adaptation of Existing Sherwood Correlations to Membrane Operations. Journal of Membrane Science, Volume 30, Issue 2, February 1987, Pages 153-170. https://doi.org/10.1016/S0376-7388(00)81349-6.

Govorov A.O. and H.H. Richardson. 2007. Generating Heat with Metal Nanoparticles. *Nano Today. Volume 2, Issue 1, February 2007, Pages 30-38.* doi:10.1016/S1748-0132(07)70017-8.

Halas N and Li Q. 2015. Thrust 2 Presentation at National Science Foundation Nanotechnology Enabled Water Treatment Engineering Research Center Kickoff Meeting.Rice University. October 21-22, 2015. http://www.newtcenter.org/.

Hu L., S. Gao, X. Ding X, et al. 2015. Photothermal-Responsive Single-Walled Carbon Nanotube-Based Ultrathin Membranes for On/Off Switchable Separation of Oil-in-Water Nanoemulsions. 15 May 26;9(5):4835-42. doi:10.1021/nn5062854.

Huysmans M and A. Dassargues. 2005 Review of the Use of Péclet Numbers to Determine The Relative Importance of Advection and Diffusion in Low Permeability Environments. Hydrogeology Journal. October 2005, Volume 13, Issue 5-6, pp 895-904. doi:10.1007/s10040-004-0387-4.

Jain P.K., X. Huang, I.H. El-Sayed, and M.A. El-Sayed. 2008. Noble Metals on the Nanoscale: Optical and Photothermal Properties and Some Applications in Imaging, Sensing, Biology, and Medicine. Accounts of Chemical Research. 41(12):1578-1586. doi:10.1021/ar7002804.

Jiang R., S. Cheng, L. Shao, Q. Ruan, and J. Wang. 2013. Mass-Based Photothermal Comparison Among Gold Nanocrystals, PbS Nanocrystals, Organic Dyes, and Carbon Black. Journal of Physical Chemistry. C 2013;117(17):8909-8915. doi:10.1021/jp400770x.

Karlsson H.O.E. and G.Trägårdh. 1996. Heat transfer in pervaporation. Journal of Membrane Science. Volume 119, Issue 2, 16 October 1996, Pp 295-30. doi:10.1016/0376-7388(96)00150-0.

Korin E., I. Ladizhensky, and E. Korngold. 1996. Hydrophilic Hollow Fiber Membranes for Water Desalination by the Pervaporation Method. Chemical Engineering and Processing: Process Intensification .Volume 35, Issue 6, December 1996, Pp 451-457. doi:10.1016/S0255-2701(96)04157-8.

Korngold E., E. Korin, and I. Ladizhensky. 1996. Water Desalination by Pervaporation with Hollow Fiber Membranes. Desalination Volume 107, Issue 2, October 1996, Pp 121-129. doi:10.1016/S0011-9164(96)00157-9.

Kreiter R., D.P. Wolfs, C.W.R. Engelen, et al. 2008. High-Temperature Pervaporation Performance of Ceramic-Supported Polyimide Membranes in the Dehydration of Alcohols. Journal of Membrane Science 319(1-2):126-132.·doi:10.1016/j.memsci.2008.03.026.

Kuznetsov Y.P., E.V Kruchinina, Y.G. Baklagina, A.K. Khripunov, and O.A. Tulupova. 2007. Deep Desalination of Water by Evaporation through Polymeric Membranes. Russian Journal of Applied Chemistry. May 2007, Volume 80, Issue 5, pp 790-798. doi:10.1134/S1070427207050199.

Kuhn J., R. Stemmer, F. Kapteijn, et al. 2009. A Non-Equilibrium Thermodynamics Approach to Model Mass and Heat Transport for Water Pervaporation Through a Zeolite Membrane. Journal of Membrane Science 330(1-2):388-398 · March 2009. doi:10.1016/j.memsci.2009.01.019.

Le N.L., Y. Wang, and T-S. Chung. 2011. Pebax/POSS Mixed Matrix Membranes for Ethanol Recovery from Aqueous Solutions via Pervaporation. Fuel and Energy Abstracts 379(1):174-183. September 2011. doi:10.1016/j.memsci.2011.05.060.

Li Q, J. Wu, N.J. Halas, et al. 2016. Use of Surface Modified Porous Membranes for Fluid Distillation. 2016. Pub. No.: WO/2016/054643. International Application No.: PCT/US2015/054028. Publication Date: 07.04.2016. International Filing Date: 05.10.2015. https://patentscope.wipo.int/search/en/detail.jsf?docId=WO2016054643.

Li Y., T. Verbiest, R. Strobbe, and I.F.J. Vankelecom. 2013. Improving the Performance of Pervaporation Membranes Via Localized Heating through Incorporation of Silver Nanoparticles. Journal of Materials Chemistry A. Issue 47, 2013. doi:10.1039/c3ta13197a.

Li Y., T. Verbiest, R. Strobbe, and I.F.J. Vankelecom. 2014. Silver Nanoparticles as Localized "Nano-Heaters" Under LED Light Irradiation to Improve Membrane Performance. *J* Journal of Materials Chemistry A. Issue 9. 3182. doi:10.1039/c3ta14406b.

Liang B., K. Pan, L. Li, E.P. Giannelis, and B. Cao. 2014. High Performance Hydrophilic Pervaporation Composite Membranes for Water Desalination. Desalination 347:199-206. doi:10.1016/j.desal.2014.05.021.

Liang B., W. Zhan, G. Qi, et al. 2015. High Performance Graphene Oxide/Polyacrylonitrile Composite Pervaporation Membranes for Desalination Applications. Journal of Materials Chemistry A. Issue 9. 5140-5147. doi:10.1039/C4TA06573E.

Lin C.X., L.P. Ding, S.Smart, and J.C. da Costa. 2012. Cobalt Oxide Silica Membranes for Desalination. Journal of Colloid Interface Science. 2012;368(1):70-76. doi:10.1016/j.jcis.2011.10.041.

Lukianova-Hleb E., Y. Hu, L. Latterini, et al. 2010. Plasmonic Nanobubbles as Transient Vapor Nanobubbles Generated Around Plasmonic Nanoparticles. ACS Nano 2010; 4(4):2109-2123. doi:10.1021/nn1000222.

Malekpour A., A. Samadi-Maybodi, and M.R. Sadati. 2011. Desalination of Aqueous Solutions by LTA and MFI Zeolite Membranes Using Pervaporation Method. Brazilian Journal of Chemical Engineering. 2011 Volume 28, Number 4, Pages 669-677. doi:10.1590/S0104-66322011000400012.

Martinez-Diez L. and M.I. Vazquez-Gonzalez. 1999. Temperature and concentration polarization in membrane distillation of aqueous salt solutions. Journal of Membrane Science 156 (1999) 265-273.

Miyawaki O., A. Saito, T. Matsuo, and K. Nakamura. 1997. Activity and Activity Coefficient of Water in Aqueous Solutions and Their Relationships with Solution Structure Parameters. Bioscience, Biotechnology, and Biochemistry.Volume 61, Issue 3, Pages 466-469. doi:10.1271/bbb.61.466.

Mulder M.H.V., J.O. Hendrickman, H. Hegeman, and C.A. Smolders. 1983. Ethanol-Water Separation by Pervaporation. Journal of Membrane Science and TechnologyVolume 16. Pages 269-284. doi:10.1016/S0376-7388(00)81315-0.

Naim M., M. Elewa, A. El-Shafei, and A. Moneer. 2015. Desalination of Simulated Seawater by Purge-Air Pervaporation Using an Innovative Fabricated Membrane. Water Science and Technology. Volume 72, Issue 5, Pp 785-793. doi:10.2166/wst.2015.277.

Neumann O., A.S. Urban, J. Day, S. Lal, P. Nordlander, and N.J. Halas. 2013. Solar Vapor Generation Enabled by Nanoparticles. ACS Nano. Volume 7, Issue 1, Pp 42-49. doi:10.1021/nn304948h.

Nicholls P. 1922. Eugene Peclet as Heating andVentilating Engineer. Journal of American Society of Heat and Ventilating Engineers. Volume 28, Issue 7, Pages 709-718.

Nieto C., H. Power, and M. Giraldo. 2014. A Boundary Integral Equation Formulation for the Thermal Creep Gas Flow at Finite Peclet Numbers. International Journal of Mechanical Sciences Volume 88, Pp 267-275. doi:10.1016/j.ijmecsci.2014.05.016.

Peng P., B. Shi, and Y. Lan. 2010. A Review of Membrane Materials for Ethanol Recovery by Pervaporation. Separation Science and Technology. Volume 46, 2010 - Issue 2, Pp 234-246. doi:10.1080/01496395.2010.504681.

Politano A., P. Argurio, G. Di Profio, et al. 2017. Photothermal Membrane Distillation for Seawater Desalination. *Advanced Materials. Volume 29, Issue 2.* doi:10.1002/adma.201603504.

Raghunath B and S-T. Hwang. 1992. Effect of Boundary Layer Mass Transfer Resistance in the Pervaporation of Dilute Organics. Journal of Membrane Science. Volume 65, Issues 1–2, 1 January 1992, Pp 147-16. doi:10.1016/0376-7388(92)87061-2.

Russell A. 2012. Plasmonic Pervaporation via Gold Nanoparticle- Functionalized Nanocomposite Membranes. PhD. Thesis. University of Arkansas, Fayetteville, Arkansas. http://scholarworks.uark.edu/etd/476/.

She M. and S-T. Hwang. 2004. Concentration of Dilute Flavor Compounds by Pervaporation: Permeate Pressure Effect and Boundary Layer Resistance Modeling. Journal of Membrane Science. Volume 236, Issue 1-2, Pp 193-202. doi:10.1016/j.memsci.2004.03.014.

She M and S-T. Hwang. 2005. Effects of Concentration, Temperature, and Coupling on Pervaporation of Dilute Flavor Organics. Journal of Membrane Science. Volume 271, Issue 1, Pp16-28. doi:10.1016/j.memsci.2005.07.005.

Sheng J. and M.S. Lefebvre. 1993. Diluted Brine Concentration Process Using Membrane Pervaporation Technique: Laboratory Scale Studies. Desalination Volume 91, Issue 3, June 1993, Pp 253-263. doi:10.1016/0011-9164(93)80063-S.

Sheng J. 1994. Pilot Scale Brine Concentration Process Using Membrane Pervaporation. Journal of Membrane Science. Volume 87(1-2), Pp 31-137. doi:10.1016/0376-7388(93)E0097-W.

Shi G.M., T. Yang, and T.S. Chung. 2012. Polybenzimidazole (PBI)/zeolitic imidazolate frameworks (ZIF-8) mixed matrix membranes for pervaporation dehydration of alcohols Journal of Membrane Science. 415-416:577-586. doi:10.1016/j.memsci.2012.05.052.

Stumm W. and Morgan J.J. 1996. Aquatic Chemistry 3rd edition, 1996, John Wiley & Sons, Inc. New York

Swenson P., B. Tanchuk, A. Gupta, and S.M. Kuznicki. 2011. Pervaporative Desalination of Water Using Natural Zeolite Membranes. Desalination. Volume 285, Pp 68-72. doi:10.1016/j.desal.2011.09.035.

Tarquin A. and G. Delgado. 2012. (378a) Concentrate Enhanced Recovery Reverse Osmosis: A New Process for RO Concentrate and Brackish Water Treatment. In: Concentrate Enhanced Recovery Reverse Osmosis: A New Process for RO Concentrate and Brackish Water Treatment. AIChE Annual Meeting. Recent Advances in Membrane-Based Brine Minimization Technologies. October 30, 2012.

Vanherck K., S. Hermans, T. Verbiest, and I. Vankelecom. 2011 (Localized Heating). Using the Photothermal Effect to Improve Membrane Separations Via Localized Heating. *Journal of Materials Chemistry. Issue 16.*

Vanherck K., I. Vankelecom, and T. Verbiest. 2011 (Photothermal). Improving Fluxes of Polyimide Membranes Containing Gold Nanoparticles by Photothermal Heating. Fuel and Energy Abstracts 373(1):5-13 . doi:10.1016/j.memsci.2011.02.010.

Wijmans J.G. and R.W. Baker. 1995. The Solution-Diffusion Model: A Review. Journal of Membrane Science. Volume 107, Issues 1–2, 15 November 1995, Pp 1-21. doi:10.1016/0376-7388(95)00102-I.

Wijmans J.G., A.L. Athayde, R. Daniels, J.H. Ly, H.D. Kamaruddin, and I Pinnau. 1995. The Role of Boundary Layers in the Removal of Volatile Organic Compounds from Water by Pervaporation. Journal of Membrane Science. Volume 109, Issue 1, 10 January 1996, Pp 135-146. https://doi.org/10.1016/0376-7388(95)00194-8.

Wynn N.P. 2003. Pervaporation. In: John Wiley & Sons, Inc., ed. Kirk-Othmer Encyclopedia of Chemical Technology. Hoboken, New Jersey, USA: John Wiley & Sons, Inc.; 2000. doi:10.1002/0471238961.1605182223251414.a01.

Xie Z., M. Hoang, T. Duong, et al. 2011. Sol–gel Derived Poly(Vinyl Alcohol)/Maleic Acid/Silica Hybrid Membrane for Desalination by Pervaporation. Journal of Membrane Science. Volume 383, Issue 1-2, Pp 96-103. doi:10.1016/j.memsci.2011.08.036.

Yacou C., S. Smart, and J.C. Diniz da Costa. 2015. Mesoporous TiO_2 Based Membranes for Water Desalination and Brine Processing. Separation and Purification Technology. Volume 147, Pp 166-171. doi:10.1016/j.seppur.2015.04.028.

Yadav A., M.L. Lind, X. Ma, and Y.S. Lin. 2013. Nanocomposite Silicalite-1/Polydimethylsiloxane Membranes for Pervaporation of Ethanol from Dilute Aqueous Solutions. Industrial and Engineering Chemistry Research. Volume 52, Issue 14, Pages 5207-5212. doi:10.1021/ie303240f.

Zwijnenberg H.J., G.H. Koops, and M. Wessling. 2005 Solar Driven Membrane Pervaporation for Desalination Processes. *Journal of Membrane Science. Volume* 250, Issue 1-2, Pp 35-246.

Zhou C., J. Zhou, and A. Huang. 2016 Seeding-free Synthesis of Zeolite FAU Membrane for Seawater Desalination by Pervaporation. Microporous and Mesoporous Materials Volume 234, Pp 377-383. doi:10.1016/j.micromeso.2016.07.050.